DESIGN AND DEVELOPMENT OF WGS CATALYSTS FOR SMALL SCALE HYDROGEN PRODUCTION UNITS

by

Coşar Doğa Demirhan

B.S., Chemical Engineering, Boğaziçi University, 2013

Submitted to the Institute for Graduate Studies in
Science and Engineering in partial fulfillment of
the requirements for the degree of
Master of Science

Graduate Program in Chemical Engineering
Boğaziçi University
2015

DESIGN AND DEVELOPMENT OF WGS CATALYSTS FOR SMALL SCALE HYDROGEN PRODUCTION UNITS

APPROVED BY:

Prof. Ahmet Erhan Aksoylu ……
(Thesis Supervisor)

Prof. Ramazan Yıldırım ……..……

Assoc. Prof. Hasan Bedir …..……

DATE OF APPROVAL: 22.07.2015

to my family and friends

ACKNOWLEDGEMENTS

First, I would like to thank my thesis supervisor Prof. Ahmet Erhan Aksoylu, who guided me throughout my thesis. It was a priviledge to work with him and I learned a lot from his wisdom and expertise in catalysis, reaction engineering.

I would like to express my sincere appreciations for the members of my thesis committee, Prof. Ramazan Yıldırım and Assoc. Prof. Hasan Bedir, for devoting their valuable time to attend my thesis defence. Special thanks to Assoc. Prof. A. Kerem Uğuz and Assoc. Prof. Ahmet Kerim Avcı for their support during both my undergraduate years and my endevours for a Ph.D. position abroad.

I wish to express my gratitude to Burcu Selen Çağlayan who deserve special thanks not only for her expertise and efforts in XPS and Raman Spectroscopy analyses, but also for her help and guidance throughout my work.

I would like to thank my dearest and lovely friends Elif Erdinç, Özgür Yaşar Çağlar, Barış Burnak, Salih Emre Demirel, Manouchehr Nadjafi, Elif Can, Elif Gençtürk, Begüm Alaybeyoğlu, and the mighty Serhat Erşahin. Thanks to their everlasting friendship and general awesomeness, my masters studies turned out to be an unforgettable, “too good to be true” experience. Without doubt, their intimate friendship was the most valuable gain of these two years.

Heartfelt thanks are for my once TA’s and now (I am proud to call) friends Kerem Aksakal, Melek Selcen Başar, Utku Deniz, Can Ekici, Merve Eropak, Burcu Karagöz, Onur Kavaklı, Sinan Koç, Aybüke Leba, Aysun İpek Paksoy, İrem Şen, and Ali Uzun. Another acknowledgement goes to my graduate classmates Serhat Arca, Hazal Bal, Özge Ertem, Çağla Odabaşı, Serdar Önsezen, and Özgü Özer. Their friendships and the countless good memories we shared will long be remembered.

Cordial thanks for Bilgi Dedeoğlu for his craftsmanship in constructing my reactor/furnace system and his technical assistance, Yakup Bal for his companionship during

our visits to various industrial areas of Istanbul, Aybars Toplu for his help with my problematic destop computer, Murat Düzgünoğlu, Melike Gürbüz, Başak Ünen, and Belkin Balkan for helping me whenever I needed. I should also thank Bilge Gedik Uluocak for her significant effort in SEM analyses and Erkan Karabekmez for his help in XRD analyses that were conducted at Boğaziçi University Advanced Technologies Research and Development Center.

Finally, I would like to express my dearest thanks to my beloved family for their patience, encouragement, and support not just for the past two years but for my whole life. Their endless love and trust in me provided me the courage to follow my dreams and desires.

Financial support for this study was provided by TÜBİTAK through project 214M170. The graduate scholarship provided by TÜBİTAK for my M.S. studies also deserves thankful recognition.

ABSTRACT

DESIGN AND DEVELOPMENT OF WGS CATALYSTS FOR SMALL SCALE HYDROGEN PRODUCTION UNITS

The aim of this work is to design and develop Au-based catalysts that suppress secondary methanation activity and show high WGS activity and stability. In this context trimetallic Au-Re-V/CeO_2 catalysts were prepared, characterized, and tested for their WGS performance. Au- and Re-loadings were kept fixed at 1 and 0.5 wt%, respectively, while V-loading levels were chosen as 0.5, 1, and 3 wt%. Performance tests were conducted under flow of ideal and realistic feed compositions, with high and low H_2O/CO ratios, at the temperature range of 250-400 °C with GHSV fixed at 120,000 ml g_{cat}^{-1} h^{-1}. Freshly reduced and spent catalysts were characterized by SEM-EDX, XPS, XRD, and Raman spectroscopy analyses. The performance test results showed that increasing V-loading in Au-Re-V system gradually decreased WGS activity and stability. Among three catalysts, 1Au-0.5Re-0.5V/CeO_2 prevailed with the highest WGS activity and stability. Higher H_2O/CO feed ratio in ideal feed increased WGS activity at high temperature. Catalysts with 0.5 and 1 wt% V-loading produced additional H_2 under realistic feed compositions. SEM-EDX analysis showed that low V-loadings yielded high Au and Re dispersions; whereas, 3 wt% V-loading resulted in formation of large size Au clusters, which were responsible for the low activity of the catalyst. XPS analysis indicated that Ce^{3+} content increased during reaction as a consequence of high WGS activity. Significant increase in Ce^{3+} content at high temperature and under flow of high H_2O/CO ratio feed suggested involvement of Ce^{3+} ions in H_2O activation. Lower V-loading resulted in higher Ce^{3+} content. XRD results suggested possible interation between V and CeO_2 that changed CeO_2 crystalline size. Combined evaluation of XPS and Raman spectroscopy results showed that V_2O_5 and $CeVO_4$ formations were present on the catalyst. Raman spectroscopy also spotted coke formation on some spent catalysts implying that deactivation via depletion of surface oxygen might be of concern.

ÖZET

KÜÇÜK ÖLÇEKLİ HİDROJEN ÜRETİM ÜNİTELERİNE YÖNELİK WGS KATALİZÖRLERİNİN TASARIMI VE GELİŞTİRİLMESİ

Bu çalışmanın amacı ikincil metanasyon aktivitesini baskılayıp yüksek gaz-buhar geçiş (WGS) aktivitesi ve stabilitesi gösterecek Au-bazlı katalizörler tasarlamak ve geliştirmektir. Bu bağlamda üç metalli Au-Re-V/CeO_2 katalizörleri hazırlanarak karakterizasyonları yapılmış ve reaksiyon performansları incelenmiştir. Au ve Re yüklemeleri sırasıyla kütlece %1 ve %0,5 olarak sabit tutulurken, kütlece %0,5, %1 ve %3 V yüklemeleri yapılmıştır. Performans testleri az ve çok H_2O/CO oranlı, ideal ve gerçekçi besleme kompozisyonlarıyla, 250-400 °C sıcaklık aralığında ve 120,000 ml g_{cat}^{-1} h^{-1} besleme hızının katalizör miktarına oranında gerçekleştirilmiştir. İndirgenmiş ve kullanılmış katalizörler SEM-EDX, XPS, XRD, and Raman spektroskopisi ile analiz edilmiştir. Performans testleri artan V yüklemesinin Au-Re-V sisteminin WGS aktivitesini ve stabilitesini düşürdüğünü göstermiştir. Üç katalizör arasında 1Au-0,5Re-0,5V/CeO_2 en yüksek WGS aktivite ve stabilitesini göstererek ön plana çıkmıştır. Yüksek H_2O/CO oranlı ideal beslemeler yüksek sıcaklıktaki WGS aktivitesini yükseltmiştir. %0,5 ve %1 V yüklemeli katalizörler gerçekçi besleme kompozisyonlarında ek hidrojen üretmiştir. SEM-EDX analizi düşük V yüklemelerinin, yüksek Au ve Re dağılımını sağladığını gösterirken; %3 V yüklemesinin katalizörün düşük performansına yol açan büyük Au kümeleri oluşumuna yol açtığı gözlenmiştir. XPS analizinde, yüksek WGS aktivitesinin reaksiyon esnasında Ce^{3+} içeriğini arttırdığı görülmüştür. Yüksek sıcaklık ve yüksek H_2O/CO oranlı ideal beslemede altındaki ciddi Ce^{3+} içeriği artışı Ce^{3+} iyonlarının su aktivasyonundaki rolünün göstermektedir. Düşük V yüklemelerinde Ce^{3+} içeriği daha yüksektir. XRD sonuçları olası V ve CeO_2 etkileşiminin CeO_2 kristal boyutunu değiştirdiğini işaret etmektedir. XPS ve Raman spektroskopisi sonuçları beraber incelendiğince katalizör üzerinde V_2O_5 ve $CeVO_4$ oluşumları görülmüştür. Bazı kullanılmış numunelerin Raman spektroskopisinde görülen karbon oluşumu yüzey oksijenlerinin tüketilmesinden kaynaklanan deaktivasyonu işaret ediyor olabilir.

TABLE OF CONTENTS

ACKNOWLEDGEMENTS iv
ABSTRACT vi
ÖZET vii
LIST OF FIGURES x
LIST OF TABLES xiii
LIST OF SYMBOLS xvi
LIST OF ACRONYMS/ABBREVIATIONS xv
1. INTRODUCTION 1
2. LITERATURE SURVEY 4
2.1. Decentralized Energy Production Systems 4
2.2. Fuel Processors: Reactions and Catalyst Requirements 5
2.3. Water-Gas Shift Reaction 7
2.3.1. General Information on the Reaction 7
2.3.2. Fuel Processor Performance of Conventional Cu-based Catalysts..... 9
2.3.3. Platinum-Group Metal Catalysts in WGS Reaction 10
2.4. Gold-based PGM Catalysts in WGS Reaction 12
2.4.1. Applications 12
2.4.2. Ceria as a Reducible Oxide Support 14
2.4.3. Rhenium Addition to WGS Catalysts 15
2.4.4. Vanadium Addition to WGS Catalysts 17
3. EXPERIMENTAL WORK 19
3.1. Materials 19
3.1.1. Chemicals 19
3.1.2. Gases and Liquids 19
3.2. Experimental Systems 20
3.2.1. Catalyst Preparation Systems 21
3.2.2. Catalyst Characterization Systems 22
3.2.3. Catalytic Reaction System for WGS Reaction 23
3.2.4. Product Analysis System for WGS Reaction 25

3.3. Catalyst Preparation and Pretreatment Procedures 25
3.4. Performance Tests 27
4. RESULTS AND DISCUSSIONS 30
4.1. WGS Performance Tests 30
4.1.1. Ideal Feed Tests 31
4.1.2. Realistic Feed Tests 36
4.2. Catalyst Characterization 41
4.2.1. SEM-EDX 41
4.2.2. XPS 44
4.2.3. XRD 51
4.2.4. Raman Spectroscopy 53
5. CONCLUSIONS AND RECOMMENDATIONS 56
5.1. Conclusions 56
5.2. Recommendations 57
APPENDIX A: TIME-ON-STREAM ACTIVITY DATA 58
REFERENCES 62

LIST OF FIGURES

Figure 3.1. Schematic diagram of the impregnation system. 21

Figure 3.2. Schematic diagram of the deposition precipitation system. 21

Figure 3.3. Schematic diagram of the microreactor flow system. 24

Figure 4.1. Temperature dependence of the catalytic activity for ideal feed # 1 (3 % CO, 15 % H_2O, 82 % Ar; H_2O/CO = 5). 32

Figure 4.2. Temperature dependence of the catalytic activity for ideal feed # 2 (3 % CO, 6 % H_2O, 91 % Ar; H_2O/CO = 2). 33

Figure 4.3. Effect of H_2O/CO feed ratio on the catalytic activity of 1Au-0.5Re-1V/CeO_2. 34

Figure 4.4. Effect of H_2O/CO feed ratio on the catalytic activity of 1Au-0.5Re-0.5V/CeO_2. 34

Figure 4.5. Effect of V-loading on the activity for ideal feed #1 at 400 ºC (3 % CO, 15 % H_2O, 82 % Ar; H_2O/CO = 5). 36

Figure 4.6. Temperature dependence of (a) catalytic activity and (b) net H_2 production for realistic feed # 1 (4.9 % CO, 32.7 % H_2O, 30.0 % H_2, 10.4 % CO_2, 22.0 % Ar; H_2O/CO = 6.7). 38

Figure 4.7. Temperature dependence (a) catalytic activity and (b) net H_2 production for realistic feed # 2 (2.1 % CO, 34.1 % H_2O, 23.7 % H_2, 12.3 % CO_2, 27.8 % Ar; H_2O/CO = 16.2). 40

Figure 4.8. SEM bright area images of freshly reduced catalysts (100000x) for (a) 1Au-0.5Re-0.5V/CeO_2, (b) 1Au-0.5Re-1V/CeO_2, and (c) 1Au-0.5Re-3V/CeO_2. 42

Figure 4.9. SEM bright area images of spent 1Au-0.5Re-0.5V/CeO_2 catalysts (100000x) for (a) realistic feed #1 and (b) realistic feed #2. 43

Figure 4.10. Mapping of freshly reduced 1Au-0.5Re-0.5V/CeO_2 catalyst. 44

Figure 4.11. XP spectra of Ce 3d region of freshly reduced catalyst samples (v: Ce^{3+}, u: Ce^{4+}). 45

Figure 4.12. XP spectra of Ce 3d region of freshly reduced and spent (ideal feed #1, 400 °C) catalyst samples with different V-loadings. 46

Figure 4.13. XP spectra of V 2p region of freshly reduced and spent (ideal feed #1, 400 °C) catalyst samples with different V-loadings. 49

Figure 4.14. XP spectra of O 1s region of freshly reduced and spent (ideal feed #1, 400 °C) catalyst samples with different V-loadings. 51

Figure 4.15. XRD spectra of the samples. 52

igure 4.16. Raman spectra of freshly reduced and spent catalyst samples with different V-loadings. 54

Figure 4.17. Raman spectra of spent 1Au-0.5Re-0.5V/CeO_2 catalyst samples indicating coke formation. 55

Figure A.1. Temperature dependence of time-on-stream activity data of 1Au-0.5Re-1V/CeO_2 for ideal feed #1. 58

Figure A.2. Temperature dependence of time-on-stream activity data of 1Au-0.5Re-1V/CeO_2 for ideal feed #2. 58

Figure A.3. Temperature dependence of time-on-stream activity data of 1Au-0.5Re-1V/CeO_2 for realistic feed #1. 59

Figure A.4. Temperature dependence of time-on-stream activity data of 1Au-0.5Re-1V/CeO_2 for realistic feed #2. 59

Figure A.5. Temperature dependence of time-on-stream activity data of 1Au-0.5Re-0.5V/CeO_2 for ideal feed #1. 60

Figure A.6. Temperature dependence of time-on-stream activity data of 1Au-0.5Re-0.5V/CeO_2 for ideal feed #2. 60

Figure A.7. Temperature dependence of time-on-stream activity data of 1Au-0.5Re-0.5V/CeO_2 for realistic feed #1. 61

Figure A.8. Temperature dependence of time-on-stream activity data of 1Au-0.5Re-0.5V/CeO_2 for realistic feed #2. 61

LIST OF TABLES

Table 3.1. Chemicals used in catalyst preparation. 19

Table 3.2. Specification and application of the liquid used. 20

Table 3.3. Specifications and application area of the gases used. 20

Table 3.4. Reactant and product gas analysis conditions. 25

Table 3.5. List of Au-Re-V/CeO_2 trimetallic catalysts. 27

Table 3.6. Ideal feed compositions used in the current study. 27

Table 3.7. Realistic feed compositions used in the current study. 28

Table 3.8. Summary of the performed experiments. 28

Table 4.1. Effect of V-loading on Ce^{3+} contents (%) of the freshly reduced and spent catalyst samples; (ideal feed #1, and 400 °C). 47

Table 4.2. Ce^{3+} content (%) of 1Au-0.5Re-0.5V/CeO_2 samples for all reaction conditions; freshly reduced and spent. 48

Table 4.3. CeO_2 lattice constants and crystallite sizes of reduced samples. 53

LIST OF SYMBOLS

a	Lattice constant
D	Disordered structural mode of crystalline carbon species
G	Graphitic carbon band with high degree of symmetry
K	Shape factor
K_{eq}	Equilibrium constant
n	Molar flow rate
$n_{H_2,in}$	Molar flow rate of H_2 in feed
$n_{H_2,out}$	Molar flow rate of H_2 in product
$n_{CO,in}$	Molar flow rate of CO in feed
$n_{CO,out}$	Molar flow rate of CO in product
P	Pressure
R	Universal gas constant
T	Temperature
V_{gas}	Volumetric flow rate of the gas
wt	Weight
β	Line broadening at half the maximum intensity
ΔH°_{298}	Standart enthalpy of reaction
λ	X-ray wavelength
θ	Bragg angle
τ	Mean size of the crystallites

LIST OF ACRONYMS/ABBREVIATIONS

BOS	Birleşik Oksijen Sanayi
BSE	Back Scattering Electron
DE	Decentralized Energy
DSS	Daily Start-Up and Shut-Down
EDX	Energy Dispersive X-Ray
EXAFS	Extended X-Ray Absorption Fine Structure
FC	Fuel Cell
FP	Fuel Processor
FTIR	Fourier Transform Infrared Spectroscopy
GC	Gas Chromatograph
GHSV	Gas Hourly Space Velocity
HPLC	High Performance Liquid Chromatography
HRTEM	High-Resolution Transmission Electron Microscopy
HSA	High Surface Area
HTS	High Temperature Shift
ICE	Internal Combustion Engine
IPCC	Intergovernmental Panel on Climate Change
IR	Infrared Spectroscopy
LNG	Liquefied Petroleum Gas
LSA	Low Surface Area
LTS	Low Temperature Shift
LT-WGS	Low Temperature Water-Gas Shift
MFC	Mass Flow Controller
MOF	Metal-Organic Framework
NCCs	Nitrogen-Containing Compounds
OD	Outer Diameter
OSC	Oxygen Storage Capacity
PEMFC	Proton Exchange Membrane Fuel Cell
PGM	Platinum Group Metal

POX	Partial Oxidation
PROX	Preferencial CO Oxidation
PSA	Pressure Swing Adsorption
SE	Secondary Electron
SEM	Scanning Electron Microscopy
SR	Steam Reforming
TCD	Thermal Conductivity Detector
TOF	Turn-over Frequency
TOS	Time-on-stream
WGS	Water-Gas Shift
XANES	X-Ray Absorption Near Edge Structure
XP	X-Ray Photoelectron
XPS	X-Ray Photoelectron Spectroscopy
XRD	X-Ray Diffraction

1. INTRODUCTION

85% of the total energy requirement of the world is supplied by fossil based fuels, coal, oil and natural gas. This results in high amounts of CO_2 emission to the atmosphere, creating environmental problems such as global climate change, continuous rise of water-level in seas, increasing numbers of floods, storms, etc. Using hydrogen as a clean and renewable energy source can be one of the solutions of this problem (IPCC, 2007).

There are different technologies for hydrogen production, ranging from fully renewable routes, like combined use of photovoltaic cells and electrolysis, to catalytic hydrogen production from hydrocarbons in fuel processors. Since the fully renewable routes are not yet economically feasible, hydrogen production from hydrocarbons is a viable alternative (LeValley *et al.*, 2014).

Water-gas shift (WGS) reaction, first reported in 1888, is an important step in many industrial processes involving hydrogen production, such as production of ammonia, refining of petroleum, Fischer-Tropsch synthesis, etc. WGS reaction is a reversible, mildly exothermic reactions and it converts CO and H_2O into CO_2 and H_2. In high-purity hydrogen production from hydrocarbons with established distribution network, WGS reaction plays a very crucial role: it increases the yield of hydrogen production (Ratnasamy and Wagner, 2009).

WGS reaction can be utilized for different purposes. In Fischer-Tropsch and substitute natural gas syntheses, WGS reaction can be used to adjust the desired H_2/CO ratio. For fuel conversion and energy production purposes, WGS reaction can be used to increase H_2 yield while getting rid of undesired CO, which is poisonous to proton exchange membrane (PEM) type fuel cells. While the reaction remains unchanged, each purpose requires WGS catalysts having different characteristics, operating in different environments and temperature ranges (Ratnasamy and Wagner, 2009).

A large scale transformation from fossil fuel based energy production to hydrogen based energy production involves many challenges. Increasing efficiency in energy

production and distribution is one of those challenges. Development and wide use of small-scale stationary, decentralized energy (DE) production units in place of existing centralized large scale units, which allow one directional energy flow only, is considered a plausible option for industrial scale transformation. According to the DE model, by using the existing natural gas and liquefied petroleum gas (LNG) distribution infrastructure and network, hydrocarbons can be easily transported to various small-scale energy production units; there, they can be converted to high purity H_2 via fuel processors which can be used in PEM fuel cells to produce electricity. In this new model, DE production units, producing energy on-site, can be integrated to a smart grid energy distribution system, enabling bi-directional electricity flow. By this way, the energy produced, which is in form of electricity, can be sold to the grid in case of excess production (Kaundinya *et al.*, 2009).

The key unit in converting hydrocarbons to hydrogen is the fuel processor (FP). A FP conventionally has three serial catalytic units, namely a reformer, a WGS unit and a preferential CO oxidation (PROX) unit. The reformer converts the fuel to a H_2 rich mixture having CO, CO_2, water vapor and unconverted hydrocarbon; the WGS unit increases the H_2 yield while suppressing CO concentration; and PROX unit reduces the CO concentration down below 40 ppm level, which guarantees long term operational stability of the PEM fuel cell (Shekhawat *et al.*, 2011).

As WGS is the slowest reaction in fuel processing, WGS reactor constitutes the bulkiest part of the fuel processor. Since WGS is an exothermic and reversible reaction, highest H_2 yield is favored at low temperatures whereas the reaction is fast at high temperatures. Conventional fuel processors overcome this challenge by using both a high-temperature WGS, also called a high-temperature shift, (HTS) reactor operating at 310-345 °C, and a low-temperature shift (LTS) reactor operating at 190-240 °C, in series. There the catalysts used are mainly industrial ones; Fe-Cr oxides for HTS and Cu-Zn-Al_2O_3 oxides for LTS (Liu *et al.*, 2013).

As industrial WGS catalysts are not specifically designed for FP systems, their performance in small scale fuel processing is unsatisfactory. Preserving activity after repeated start-up and shut-down cycles; stable operation under feeds having oxygen and excess water; thermal stability; and low methanation activity are some of the performance

criteria for which industrial WGS catalysts fail to satisfy. An efficient and robust WGS catalyst can be the key to a successful FP operation; hence, there has been an intensive research on design and development of Platinum-group metal (PGM) based, metal oxide supported, non-pyrophoric WGS catalysts. In the literature, Au- and/or Pt-based catalysts are reported to have promising WGS performance. A single WGS reactor, which utilizes a highly active and stable catalyst, operating at HTS-LTS transition temperatures, i.e. 250-350 °C, is preferred over the conventional use of serial HTS and LTS reactors in FP operations (Castaño et al., 2014). Au/ and Au-Re/CeO_2 catalysts were extensively studied by previous members our research group and addition of Re to Au/CeO_2 system was found beneficial (Çağlayan, 2011).

The aim of the proposed work is to design and develop Au-based, CeO_2 supported trimetallic Au-Re-V catalysts that suppress secondary methanation activity, show high performance in temperature range of 250-400 °C allowing the use of a single WGS reactor in fuel processor, and to maintain high activity under water rich ideal and realistic (i.e. feed having CO, H_2O, H_2, CO_2) feeds. The performance of Au-Re system was aimed to be improved with V addition. In this context; Au-Re-V/CeO_2 catalyst with different V-loadings were developed and tested for their performance for ideal and realistic (i.e. feed having CO, H_2O, H_2, CO_2) feeds.

In the studies, catalyst composition, temperature and H_2O/CO ratio in both types of the feeds were used as the experimental parameters. Activity, selectivity, and stability for steady state operation mode were considered as the performance criteria. The microstructural properties of the samples were analyzed by SEM-EDX; the crystal formations were characterized by XRD; the oxidation states of the metals and support were determined by XPS; and possible V-O-V and V-O-Ce bonds were examined by Raman spectroscopy.

Chapter 2 involves a detailed literature survey on decentralized energy production, fuel processor processes, and water-gas shift reaction catalysts. Chapter 3 contains the details of the experimental work carried out. The results obtained in the performance and characterization tests are discussed in Chapter 4 and the conclusions of the current study and recommendations for the future work are presented in Chapter 5.

2. LITERATURE SURVEY

2.1. Decentralized Energy Production Systems

World's energy production is highly dependent on combustion of fossil fuels. In its 2007 report, Intergovernmental Panel on Climate Change (IPCC) stated that 85 % of total energy requirement of the world is produced by using coal, oil, and natural gas (IPCC, 2007). Fossil fuels are energy-rich materials owing to their high hydrocarbon content; however, they pose a great threat to environment; high amount of carbon dioxide (CO_2), which is the product of combustion, emitted to the atmosphere creates environmental problems such as global climate change, continuous rise of water-level in seas, increasing numbers of floods, storms, etc. (IPCC, 2007).

As an alternative to fossil fuels, hydrogen has become an important fuel and energy carrier owing to its advantages in reduction of greenhouse gas emissions, improved energy security, and increased energy efficiency. Hydrogen is already used as a feedstock for chemical processes ranging from refinery operations, such as hydrotreating and hydrocracking, to chemicals manufacturing, such as ammonia and methanol synthesis (Avcı *et al.*, 2001). A promising feature of hydrogen is that when it is fed to a fuel cell, which is an electrochemical energy production device, electricity can be produced with only water as the side product. Commercial fuel cells are available; however they require very high purity hydrogen as fuel. Challenges related with storage and distribution of hydrogen suggests that in the near future centralized production of hydrogen is not a sustainable solution. A viable option to overcome these impracticalities is the use of small-scale decentralized, on-site, hydrogen production units (Kaundinya *et al.*, 2009).

Decentralized energy (DE) production systems rely on using the well-established distribution infrastructure and network of natural gas/LPG. Instead of producing energy on large-scale and centralized units and then distributing it to highly populated regions, DE system proposes transporting the energy carrier in form of fuel to multiple small-scale energy production units and converting them to first hydrogen and then to electricity on-site. Catalytic units called fuel processors can be used for converting fuels to hydrogen rich

mixtures. Later, hydrogen is reacted with oxygen in the air in a fuel cell and electricity is produced. Thermal efficiency of the entire process is much higher than that of combustion of fossil fuels, and additionally, energy losses during transportation of electricity are minimized. By-products of energy production in a fuel cell are water and small amounts of heat. Apart from environmentally friendly aspects of combined fuel processors-fuel cell systems, DE production system supports the "smart grid" energy distribution system. Thanks to the smart grid system, when DE production units are connected to a grid, two directional electricity flow is enabled; thus, in case of excess production, electricity can be sold to the grid (Kaundinya *et al.*, 2009).

2.2 Fuel Processors: Reactions and Catalyst Requirements

Fuel cell technology is a clean alternative to the conventional internal combustion engines (ICE). This new technology does not allow any environmentally harmful emission and operates with better energy efficiency compared to that of an ICE. The main drawback of this technology is the lack of sustainable production of very high purity hydrogen. This problem can be overcome via fuel processors (FP). FPs use the hydrocarbon fuels having well established network, and convert them on-site to desired high purity hydrogen (Lenite *et al.*, 2011).

An FP consists of three catalytic units, namely a reformer, a water-gas shift (WGS) unit and a preferential CO oxidation (PROX) unit. The reformer is the first reactor in an FP. In a reformer steam reacts with hydrocarbon fuels, which is either a gas (e.g. CH_4) or a liquid (e.g. gasoline, diesel), to a mixture of H_2, CO, CO_2, water vapor, and unconverted hydrocarbons (Shekhawat *et al.*, 2011). The reaction is called steam reformation or steam reforming. Despite many alternatives, gaseous fuel reforming is currently the main source of the produced hydrogen. In 2012, 95 % of the hydrogen in the United States was produced via reformation of methane with steam (LeValley *et al.*, 2014). Steam reforming (SR) of methane reaction is given as (Ratnasamy and Wagner, 2009):

$$\mathrm{CH_4 + H_2O \leftrightarrow CO + 3H_2} \qquad \Delta H^{\circ}_{298} = 206.2\ \mathrm{kJ/mol} \tag{2.1}$$

Main advantage of SR to other hydrogen production routes is the high H_2 yield (high H_2/CO ratio) it provides. The disadvantage comes from high endothermicity of SR, which necessitates high energy input and high reaction temperatures in the range 700-1000 °C. The most widely used (and studied) SR catalysts are Ni based. They are cheap and show fairly good activity; however they are prone to serious coke formation during reaction. Using excess steam can suppress coking, but in return increase the energy demand of the process (LeValley *et al.*, 2014).

An alternative way to overcome the high energy and utility demands of the steam reforming reaction is to combine it with partial oxidation (POX) of methane (Ratnasamy and Wagner, 2009). The combination is often called as "oxidative steam reforming" and it can improve economics of the energy intensive hydrogen production at the cost of reducing H_2 yield. Pt is a successful catalyst for POX (Shekhawat *et al.*, 2011):

$$\mathrm{CH_4} + \tfrac{1}{2}\mathrm{O_2} \leftrightarrow \mathrm{CO} + 2\mathrm{H_2} \qquad \Delta \mathrm{H}^{\circ}_{298} = -35.6\ \mathrm{kJ/mol} \tag{2.2}$$

Reformer effluent stream contains significant amount of unreacted H_2O and low-to-mid amounts of CO (10-50%). The unreacted H_2O reacts with CO to produce CO_2 and additional H_2 via WGS reaction. The reaction is written as (Ratnasamy and Wagner, 2009):

$$\mathrm{CO} + \mathrm{H_2O} \leftrightarrow \mathrm{CO_2} + \mathrm{H_2} \qquad \Delta \mathrm{H}^{\circ}_{298} = -41.2\ \mathrm{kJ/mol} \tag{2.3}$$

Although plagued by a trade-off between thermodynamic limitations and slow kinetics, WGS reactors manage to reduce the amount CO to 0.5-1% levels by employing multiple reactor configurations. Industrial WGS catalysts are Fe-based for high temperature WGS and Cu-Zn-based for low temperature WGS reaction (LeValley *et al.*, 2014).

H_2 must be pure enough to be used in state-of-art polymer electrolyte membrane fuel cells (PEMFC); the CO content of the hydrogen fed to PEMFC's should be reduced to ppm levels. For Pt-Re anode electro catalyst, the CO concentration should be below 50 ppm; whereas, when Pt anode is used, CO content should be below 10 ppm (Lenite *et al.*, 2011). Reducing the CO level from 0.5-1% to 20-40 ppm can be achieved by using a PROX reactor (Ratnasamy and Wagner, 2009):

$$CO + O_2 \rightarrow CO_2 \qquad \Delta H^{\circ}_{298} = -283.6\ \mathrm{kJ/mol} \tag{2.4}$$

The drawback of PROX reaction is that the catalyst should be very selective, such that instead of oxidizing the highly concentrated H_2 in the feed, it should oxidize CO which is already at very low concentrations. This can be adjusted by carefully controlling the reaction temperature. Pt is reported to be a good candidate to be used in PROX catalysts (Çağlayan *et al*., 2011).

Alternative H_2 purification methods include membrane separation and pressure swing adsorption. Membrane separation uses high pressure gradient between two sides of a membrane to separate H_2 from CO and CO_2. The process requires high temperatures and thermal stability of up-to-date membranes are still problematic (Azzam *et al.*, 2013). Pressure swing adsorption (PSA) method relies on mostly zeolite based adsorbents to capture unwanted gas species such as CO_2. Adsorption is a dynamic process and once the adsorbent material is saturated with adsorbed gas, it must be regenerated. Continuous operation of a PSA unit can thus be carried out with two parallel units operating in a cyclic manner (Lenite *et al.*, 2011).

Challenges related with fuel processors operation are: the complications that are encountered during start-up and shut-down; the need of very low CO levels that are demanded by the fuel cell specifications; and the requirement of stable long-term operation for both stationary and (possibly) mobile applications. Studies in the literature show that there is still a large room for research and development in many areas of FP operations (LeValley et. al., 2014).

2.3. Water-Gas Shift Reaction

2.3.1. General Information on the Reaction

Water-Gas Shift (WGS) is a redox type reaction that converts water vapor and carbon monoxide into carbon dioxide and hydrogen (Ratnasamy and Wagner, 2009):

$$CO + H_2O \leftrightarrow CO_2 + H_2 \qquad \Delta H^{\circ}_{298} = -41.2\ \mathrm{kJ/mol} \tag{2.3}$$

The thermodynamic equilibrium constant (K_{eq}) for the WGS reaction is reported as function of absolute temperature (Ratnasamy and Wagner, 2009):

$$K_{eq} = [\exp(4577.8/T) - 4.33] \tag{2.5}$$

WGS is a reversible and mildly exothermic reaction. According to thermodynamics of the reaction, the equilibrium shifts to reactants side with increasing temperature, meaning reverse reaction is dominating at higher temperatures. There are thermodynamic limitations at high temperatures and kinetic limitations at low temperatures; hence in industrial applications, WGS reaction is typically performed in two consecutive stages (Lee *et al.*, 2013-Zhu *et al.*, 2011). The first stage is called high temperature shift (HTS) reaction which is performed at 350-500 °C on Fe_3O_4/Cr_2O_3 catalyst. The second stage is called low temperature shift (LTS) reaction performed at 180-240 °C on $Cu/ZnO/Al_2O_3$ catalyst.

Fe_3O_4/Cr_2O_3 and $Cu/Zn/Al_2O_3$ catalysts that are currently used in industrial operations are limited in use for fuel processor (FP) applications. The reasons are thermodynamic limitations at high temperatures, sensitivity to air and condensed vapor, the need of long pre-conditioning, and slow kinetics at low temperatures. In order to overcome these problems, there has been an extensive effort in the scientific community to come up with active, selective, thermally stable, poison resistant, and non-pyrophoric metal or noble metal based WGS catalyst formulations supported on metal oxide carriers which are suitable for FP applications (Çağlayan and Aksoylu, 2011-Liu *et al.*, 2013). There is a consensus that the resulting catalyst should be bifunctional such that the metal part should adsorb and activate CO, whereas the metal oxide support should activate H_2O (Azzam. *et al.*, 2008). Additionally, the catalyst must not favor the methanation reaction, which is the reverse reaction of steam reforming (Ratnasamy and Wagner, 2009):

$$CO + 3H_2 \leftrightarrow CH_4 + H_2O \qquad \Delta H^{\circ}_{298} = -206.2\ \mathrm{kJ/mol} \tag{2.6}$$

FP operations consist of steady-state and transient behaviors. Both mobile and stationary FP operations often require daily start-ups and shut-downs (DSS). With fast and energy efficient start-ups strategies, for instance by using reactive heating instead of

sequential heating, FP units can be heated up to required reaction conditions in under 30 minutes (Maximini *et al.*, 2014).

During DSS, the catalyst is rapidly heated up to start the reaction, works at steady-state and then it is cooled down with possible exposure to air and liquid water (Liu *et al.*, 2013). WGS catalysts, especially industrially used catalysts, are affected in negative ways during such DSS operations.

2.3.2. Fuel Processor Performance of Conventional Cu-based Catalysts

Since the Cu-based catalyst have been already used in industry for LT-WGS reactions, there are many studies on transient behavior of Cu-based catalysts (Guo *et al.*, 2009a-Guo *et al.*, 2009b-Kam *et al.*, 2010-Liu *et al.*, 2012-Nishimura *et al.*, 2010-Shishido *et al.*, 2009-Maciel *et al.*, 2013).

$Cu/ZnO/Al_2O_3$, a typical LT-WGS catalyst, was subjected to such tests, and found to be prone to continuous deactivation in shut-down and start-up operations. The reasons behind deactivation was suggested to be blocking or deterioration of the active sites by the formation of $Zn_6Al_2(OH)_{16}CO_3 \cdot 4H_2O$ species, rather than sintering, which changes the size of Cu crystallites. As a result, interface between Cu crystallites and oxides is found to have an important role in catalytic activity. This is directly related to the catalyst preparation method (Guo *et al.*, 2009a).

Effect of preparation methods and calcination temperature on activity and stability of Cu-based catalysts during steady-state and DSS operations were also investigated. Catalyst prepared by co-precipitation, homogeneous precipitation, sol-gel and impregnation methods were characterized and their performance were comparatively analyzed. In-situ formation of a small-sized surface species AlO(OH) (Boehmite) is found to have an inhibitory effect against aggregation of Cu metal leading improved sustainability against DSS operation. When prepared with co-precipitation method and calcined at 823 K, the catalyst was found to be most stable after 50 cycles of start-up and shut-down (Nishimura *et al.*, 2010).

Amount of metal loading on Cu-based catalysts is also an affecting factor on both CO conversion and catalyst deactivation. Cu/ZnO catalysts having Cu-loadings changing between 5-44 wt% were compared for their WGS performance. DSS behavior was also investigated, and sintering and crystallite size are found having insignificant effect on catalyst deactivation. For a steady-state operation, Cu-loading can be safely decreased from 44 to 25 wt% without any loss in performance. In case of DSS operations a further decrease in Cu-loading can be allowed. Catalyst with 15 wt% Cu-loading were found to be optimal; with decreasing Cu-loading, effect of pyrophoricity also lessened (Liu *et al.*, 2012).

Studies on Cu-based catalysts also include testing of different support materials. In such a study, Cu/ZnO was compared with Cu/ZnO-Al_2O_3 during DSS operations. Cu/ZnO has comparable activity to Cu/ZnO-Al_2O_3, but it is superior in terms of stability. This was attributed to presence of Al_2O_3, which is suggested to contribute to the formation of carbonate species, which block active Cu-ZnO interface sites responsible for WGS reaction (Guo *et al.*, 2009b). Another study makes a comparison of CeO_2, ZrO_2, MgO and Al_2O_3 supports. All supports were tested in a large temperature range of 200-350 °C. At 200 °C Cu/ZrO_2 was found to be the most active, whereas Cu/CeO_2 gave the highest conversion at 350 °C. All catalysts were found to be selective to CO_2, rather than H_2. Reducibility of the catalysts was found to affect activity, and co-precipitated Cu/CeO_2 showed easier reducibility, hence the highest activity and stability (Jeong *et al.*, 2014).

There are some serious drawbacks of using Cu-based catalysts. They are not very stable against oxidizing gases when compared to Pt-, Ru- or Au-based catalysts (Nishimura *et al.*, 2010). Pyrophoricity is also a problem encountered at medium to high Cu-loadings. Temperature rise of Cu-based catalysts expose to air can reach to 621 °C. This can be very problematic during DSS operations (Liu *et al.*, 2012).

2.3.3. Platinum-Group Metal Catalysts in WGS Reaction

In addition to the variations of Cu-based catalysts, Platinum group metals (PGM) on reducible and non-reducible oxides were also largely studied. Studied catalysts consist of Rh, Ru, Ir, Au, and Pd as the active metals; among those Pt has been the most investigated and the most promising precious metal for the WGS reaction (Ratnasamy and Wagner, 2009-

Gökaliler, 2013). CeO_2, ZrO_2, Al_2O_3, TiO_2, and SiO_2 were used as support material. WGS activity of Pt on CeO_2, TiO_2 and ZrO_2 supports were specifically investigated in some studies (Azzam *et al.*, 2007b). Results indicated that Pt on TiO_2 is the most active formulation among the studied catalysts. Pt/CeO_2 catalysts suffered deactivation caused by the stable carbonate species formation on the CeO_2 support. Cause of deactivation of Pt/TiO_2 was suggested to be sintering of the Pt. As the addition of Re to the Pt/TiO_2 was found to prevent Pt sintering, WGS activity could be enhanced upon Re addition (Azzam *et al.*, 2007b-Azzam *et al.*, 2008-Azzam *et al.*, 2013). Recent studies include Pt-Ni bimetallic catalysts supported on CeO_2 with high and low surface area (denoted as HSA and LSA), ZrO_2, γ-Al_2O_3, TiO_2 and SiO_2. Pt-Ni bimetallic catalysts were ranked according to their activities, based on catalyst weight, as follows: CeO_2 >HSA-ZrO_2 > TiO_2 > γ-Al_2O_3 >SiO_2 >LSA-ZrO_2. When the CO uptake values are considered, a similar ranking is valid except that Pt-Ni/TiO_2 becomes as active as Pt-Ni/CeO_2. They also compared the catalysts in terms of selectivity to CH_4, and found that Pt-Ni on TiO_2 and HSA-ZrO_2 have very low selectivity to CH_4. They concluded that CeO_2, TiO_2, and HSA-ZrO_2 are promising supports for the bimetallic Pt-Ni catalyst (Wang, *et al.*, 2013).

One comparative study (Kam *et al.*, 2010) focused on pyrophoric properties of Cu- and Pt-based catalysts. The resistance of Pt-catalysts to chlorine and sulfur poisoning was also studied. Cu/ZnO experienced more than 100 °C temperature rises during start-up and shut-down operations, whereas Pt-based catalysts showed no pyrophoricity. Pt/CeO_2 catalyst retained its activity after steady-state and DSS operation; however Pt/TiO_2 and Pt/ZrO_2 catalysts went through serious sintering during steady-state operation. Cu/ZnO catalyst lost its activity during DSS operations (Kam *et al.*, 2010).

In a study on the performance of Pt-based catalysts supported on doped CeO_2, Pt/Ti^{4+}-doped CeO_2 exhibited enhanced WGS activity compared to Pt/CeO_2 and Pt/TiO_2. The explanation was the existence of higher site reactivity (k) and a larger concentration for active “H-containing” and “C-containing” intermediates formed within a reactive zone around each Pt nanoparticle, and a larger concentration of labile oxygen and oxygen vacancies present in the Ti^{4+}-doped CeO_2 support, which participate in WGS via the “redox” mechanism. Additionally, the WGS mechanism on Pt supported on CeO_2-doped carrier (Zr^{4+}, $La^{3+}$and Ti^{4+} dopant) at 300 °C was found to proceed via the “redox” bifunctional

mechanism in parallel to the "associative mechanism with OH group regeneration" mechanism (Petallidou et al, 2014).

Activities of Pt and Au catalysts were compared and summarized in a very recent study. Au-based catalysts have superior activity at low temperatures, such as 180 °C, whereas Pt-based catalysts are very successful at temperatures around 250 °C, and they even attain equilibrium conversion with high TOF. Au-based catalysts are more influenced by electronic properties of the support. For both types of catalysts, CeO_2 or CeFe oxide supports were found to be beneficial for WGS activity (Castaño *et al.*, 2014).

2.4. Gold-based PGM Catalysts in WGS Reaction

2.4.1. Applications

In early studies, Au-based catalysts was considered inactive due to large Au particle size. However, when particle size of Au clusters on a support surface is below 5 nm, activity for CO conversion is observed. With the right surface configuration, Au showed high activity for CO oxidation even at temperatures around – 70 °C (Haruta *et al.*, 1989). Nano-scaled Au supported on CeO_2 shone out as a promising catalyst for WGS in numerous studies (Tabakova *et al.*, 2004-Lenite *et al.*, 2011-LeValley *et al.*, 2014). The high activity of Au/CeO_2 was attributed to the close contact between well-dispersed Au particles and the defects on the CeO_2 support surface. Long term stability was suggested to the stability of those small Au clusters on CeO_2 (Tabakova *et al.*, 2004).

Particle size of Au clusters can be modified via preparation conditions and calcination temperature. With the increase in calcination temperature from 400 to 650 °C, the average particle size increases from 4.6 to 9.2 nm (LeValley *et al.*, 2014). Many metal addition techniques were employed for Au addition on CeO_2. The listed methods were: incipient-to-wetness impregnation, co-precipitation, co-sputtering, deposition-precipitation, gas/liquid phased grafting, and combustion. Among those methods, deposition-precipitation and co-precipitation were compared (Tabakova *et al.*, 2004), and the former proved to be superior as it yielded narrower particle size distribution and Au deposited on the surface of the

support. Also, well-crystallized CeO_2 support resulted in higher activity compared to its amorphous and not-well crystallized state (Tabakova *et al.*, 2004).

Characteristics and performance of Au-based catalysts during daily start-up and shut-down (DSS) operations were also investigated, and severe deactivation was observed (Liu *et al.*, 2013). In the study, 1.85 % Au/CeO_2 catalyst was prepared by deposition-precipitation method. XRD results showed high Au dispersion, which ensures high activity. After few cycles of DSS, deactivation was severe. Sintering was ruled out as a source of deactivation. Formation of carbonate species on the surface was considered as a possible deactivating factor. During calcination the formed carbonate species were expected to decompose; accordingly, activity should increase after calcination. However, this was not the case; the results indicated that carbonate species were only partially responsible in catalyst deactivation. By using XPS and XANES analyses, effects of reducing gases, such as H_2 and CO, were investigated, and reduction of the catalyst was proposed as the cause of deactivation. Correspondingly, exposure to H_2O and CO_2 increased activity. Reduction of catalyst depletes the active Au-O linkages of Au-CeO_2 interface at steady-state operation. Deactivation during DSS was attributed to pure blockage of carbonates, since calcinations restored initial activity after DSS cycles. Finally, the group proposed increasing oxidizing potential of the atmosphere by adding O_2 may circumvent catalyst deactivation for steady-state operation, and performing start-ups and shut-downs in presence of H_2 or (preferably) H_2O can ensure activity (Liu *et al.*, 2013).

Au catalysts have been found attractive due to their high activities at lower temperatures. Pt-based catalysts are insufficiently active below 250 °C (Ratnasamy and Wagner, 2009). A comparative analysis of the activities of Pt and Au on ZrO_2 catalysts under typical autothermal reformer outlet conditions revealed that Au/ZrO_2 shows higher activity than Pt/ZrO_2 in the temperature range of 423-513 K (Boaro *et al.*, 2009). Au/CeO_2 was found as the most active catalyst in the range of 373-523 K among Pt/CeO_2, Au/TiO_2, $Cu/ZnO\text{-}Al_2O_3$ based on the results of the temperature-programmed reaction measurements. In the tests no methanation was observed below 623 K (Sakuari *et al.*, 2005).

2.4.2. Ceria as a Reducible Oxide Support

CeO_2 is used as a catalyst both in purification of exhaust gases in three-way automotive catalytic converters and in solid oxide fuel cells. In addition to those merits, it is a very promising metal oxide support for noble metal based catalysts. Ability of CeO_2 to easily form surface defects in forms of oxygen vacancies gives it high oxygen storage capacity (OSC), which provides high reactivity for catalytic reactions (Tabakova *et al.*, 2004-Nolan *et al.*, 2006-Campbell and Peden, 2005). The highly mobile lattice oxygen is involved in many oxidation processes (Esch *et al.*, 2005).

Defects and step edges are reported to be most reactive sites on metal oxide surfaces. A surface oxygen vacancy is created when an adsorbate is oxidized. Such a vacancy can bind to adsorbates stronger than normal oxide sites and assist their dissociation. This high reactivity of vacant sites are attributed to Ce^{3+} ions being exposed to gas phase reactants (Campbell and Peden, 2005). The excess electrons that are left behind when neutral oxygen is removed are reported to localize on empty f states of Ce ions. As a result the Ce^{4+} ions of the surface are reduced to Ce^{3+} ions. This reduction is reported to efficiently enhance the reactivity of the CeO_2 substrates (Esch *et al.*, 2005).

Another aspect of CeO_2 that makes it a promising support material for catalysts is its ability to stabilize nano-scaled noble metals against sintering and allowing them to disperse with high degree on its surface (Esch *et al.*, 2005). Since the surface defects in form of oxygen vacancies allow strong binding of catalytically active species on CeO_2, high dispersion of ionic metal species can be obtained. A good example for this property of CeO_2 is the high activity of Au/CeO_2 catalysts that was proven in various studies (Tabakova *et al.*, 2004-Esch *et al.*, 2005- Çağlayan and Aksoylu, 2011-LeValley *et al.*, 2014). Although CeO_2 has high OSC, its capacity can be further increased. Addition of Zr ions to CeO_2 was reported to increase the supports OSC (Esch *et al.*, 2005-Dutta *et al.*, 2006).

There are two reported reaction routes for WGS reaction on reducible oxide supports. First one is the redox mechanism, for which catalyst support is successively reduced by CO and oxidized by H_2O. The second route is the associate formates, where the reaction is

proposed to go through adsorbed surface formate species. The reaction route changes with the active metal, the reaction conditions, and the type of support (Azzam *et al.*, 2008).

Effect of supports on activity of the Au-based catalysts were examined in a comparative study of catalysts prepared by deposition-precipitation method on pure ceria, iron oxide and mixed Ce–Fe composite oxides, synthesized by the urea gelation co-precipitation pathway. Obtained catalysts were characterized by HRTEM, FTIR and Mossbauer spectroscopy. The impact of the support composition on the WGS reaction activity was found as: Au/CeO_2 > Au/Ce50Fe50 > Au/Ce75Fe25 > Au/Ce25Fe75 > Au/Fe_2O_3. This effect was attributed to significant differences in Au particle size and the ability of the supports to assist formation of oxygen vacancies formation. Au particle size appeared more decisive factor for the activity of Au/CeO_2 and Au/Fe_2O_3, while the structural properties of mixed oxide supports, particularly the presence of Ce^{3+} defects and oxygen vacancies, controlled the performance of Au/CeO_2–Fe_2O_3 catalysts (Tabakova, *et al.*, 2011).

2.4.3. Rhenium Addition to WGS Catalysts

Pt and Re supported on Al_2O_3 has been a successful naphtha reforming catalyst since 1960's. With the emergence reducible oxide support for future catalysts, various groups tested the performance of Pt-Re supported over different reducible oxide supports in WGS reaction (Iida and Igarashi, 2006-Azzam *et al.*, 2008-Azzam *et al.*, 2013).

Iida and friends reported that Re addition increased dispersion of Pt on TiO_2, whereas the dispersion of Pt decreased on ZrO_2. In either case strong electronic interaction between Pt and Re was observed from the XPS analysis. TiO_2 was reported to allow stronger interaction between Pt and Re compared to ZrO_2. The interaction improved the WGS activity of the catalyst. XPS results showed that oxidation states of Re changed between Re^{3+} and Re^{7+} supporting the proposed reaction mechanism (Iida and Igarashi, 2006).

Azzam *et al.* studied Pt-Re catalysts supported on reducible oxide supports such as CeO_2, ZrO_2, TiO_2, $Ce_xZr_{1-x}O_2$ and $TixCe_{1-x}O_2$. Their mechanistic studies showed that no catalyst followed redox or associative mechanism separately, but instead the mechanism

followed was dependent on the support and the experimental conditions (Azzam *et al.*, 2008).

CO and H_2O pulse experiments showed that reaction followed both mechanisms. CO pulse resulted in formation of H_2 and CO_2, which was supported by the hydroxyl groups of the catalyst surface where no formate species was observed in the FTIR results. It was suggested that ReO_x sites on catalyst surface provided additional redox routes for the WGS reaction by giving an oxygen atom to CO producing CO_2, and then reoxidized with H_2O. A temperature programmed reduction study proved that ReO_x was partially reduced at WGS reaction conditions and it was fully reduced only above 525 °C. While Re is at its partially reduced state, it still has availability to provide oxygen for the reaction (Azzam *et al.*, 2008).

A further study of the same group focused on the state of added Re and its interaction with Pt for Pt-Re/TiO_2 system. They found state of Pt and extent of Pt-Re interaction is a function of metal precursors used, preparation procedure followed, the type of the support and the corresponding metal loadings. Reduction and oxidation cycle on ReO_x was held responsible for the suggested increase in water dissociation rate (Azzam *et al.*, 2013).

Pt-Re catalysts were prepared by impregnation methods and the group studied effects of impregnation sequences on Pt metal surface area. When Re was deposited prior to Pt, the Pt metal surface area and WGS activity were higher. The catalysts prepared without an intermediary drying and calcination showed better activity and stability. Since an early EXAFS study showed that Re has higher affinity for chlorine than oxygen, the group suggested that the high performance of the catalyst is due to the type of the Pt-precursor that was used, namely aqueous H_2PtCl_6. It was argued that Re reacts with the Cl coming from from the deposited $PtCl_6^{2-}$ on TiO_2. Pt:Re molar ratio was also found to be critical in the performance level of the catalysts. When the ratio was low, number of active Pt sites for the reaction decreased and ReO_x became the significant part. Increasing the Pt:Re ratio ensured high activity (Azzam *et al.*, 2013).

A detailed FTIR study showed that the addition of H_2O to feed has more influence on Pt-Re catalyst than on Pt catalyst. With H_2O addition, CO peaks on Re disappeared; suggesting Re was oxidized by H_2O and thus CO adsorption was prevented. Presence of Re

on the catalyst was suggested to lower PtO_x reduction temperature. Formation of a Pt-Re alloy on the surface was speculated, however the interaction of Pt-Re was not held responsible for the high activity. An in situ IR spectroscopy proved that Re presence influenced the surface OH-groups of the catalyst. Hence, the group concluded that the ability of ReO_x to provide additional route for redox mechanism was the only candidate for the high activity and stability (Azzam *et al.*, 2013).

Çağlayan and Aksoylu have studied effect of Re addition on Au/CeO_2 catalysts. In their study, the optimum formula was found when very small amount of Re was impregnated on CeO_2 and then Au was added via deposition precipitation method. No calcination step between two metal additions was performed. HRTEM results showed that this allowed for surface alloy formation which resulted in conversions near the equilibrium levels for ideal feed conditions. In addition to the high activity, additional H_2 production was observed over $1Au\text{-}0.5Re/CeO_2$ catalyst for high H_2O/CO feed ratios in the real feed. Re was found to have a stabilizing effect on the formate species and accelerated the rate of hydrogen formation (Çağlayan and Aksoylu, 2011). XPS results suggested that that high activity was related with the high Ce^{3+} content, which then allowed enhanced electron transfer ability from support to metallic sites (Tabakova *et al.*, 2004-Çağlayan and Aksoylu, 2011).

A further study of the same group investigated the kinetics of WGS over $Au\text{-}Re/CeO_2$. The resulting rate orders indicated that at high temperatures surface coverage of CO is low and addition of Re reportedly increase the water activation ability of the catalyst. As expected, presence of CO_2 and H_2 in the feed had an inhibitory effect on reaction rates due to reverse WGS reaction and competitive adsorption. Reported rate orders for CO, H_2O, CO_2, and H_2 are 0.75, 2.0, -0.34, and -0.60, respectively (Gökaliler *et al.*, 2013).

2.4.4. Vanadium Addition in WGS Reaction

Farias *et al.* performed a study focusing on adding V to the already successful Pt/CeO_2 catalyst to improve its activity and stability. V in oxide form, VO_x, is a widely used catalyst for many oxidation reactions. Additionally, V is reported to have a capacity of generating structural defects. Partially reduced V is known to present high oxygen mobility. In previous

studies of the group, V_2O_3 phase was found to be active for WGS above 450 °C (Farias *et al.*, 2008).

In the study, V was impregnated on CeO_2 by wet impregnation. The V-loading was measured as weight percent (wt%) of V_2O_5 on the catalyst, and changed between 1 and 18 wt%. BET surface area measurements show that V addition led to a decrease in surface area. $CeVO_4$ and V_2O_5 phases formed were used as the reference materials for infrared spectroscopy study. These two phases of V were also observed in the XRD analysis. The authors suggested that preparation methods and the amount of V affected dispersion and the type of vanadate species formed on the surface, respectively. V^{5+}-O-Ce^{3+} sites were developed through the ability of surface vanadium oxides to remove oxygen from the most easily reducible surface oxide, CeO_2 (Farias *et al.*, 2008).

XPS results indicated that as V loading increased, distribution of oxidation states on the surface became wider; hence, spectra became more complex. Observed oxidation states of V were V^{5+},V^0, V^{2+}, and V^{3+}. As the V loading decreased, formation of dispersed VO_x species were favored rather than formation of isolated or polymeric units. For Pt/1VCeO_2 (indicating 1wt% V_2O5), only V^{5+} state of V was observed. XPS results also suggested that presence of V directly influenced the distribution of Pt oxidation states (Farias *et al.*, 2008).

Among the resulting catalysts, Pt/6VCeO_2 showed the highest activity and stability over a temperature interval ranging between 200 and 350 °C. V loadings lower and higher than this value showed less activity. At this optimum surface configuration, formation of mono- and polyvanadates species were favored, which was confirmed by FTIR and XRD results. V-O-V bonds were found to be inactive in WGS reaction; whereas, V-O-Ce bonds were suggested to promote WGS activity when slightly below monolayer coverage of the surface V species was obtained (Farias *et al.*, 2008).

Garcia *et al.*'s recent study on physically mixed V_2O_5 and Au/TiO_2 catalyst showed that the mixture has higher activity in oxidative dehydrogenation of propane than those over both catalysts individually. However, the group suggested that V sites were only active for propane activation and Au/TiO_2 was solely responsible for the high WGS activity (Garcia *et al.*, 2015).

3. EXPERIMENTAL WORK

3.1. Materials

3.1.1. Chemicals

All the chemicals used for catalyst preparation are presented in Table 3.1.

Table 3.1. Chemicals used in catalyst preparation (all specifications: research grade).

Chemicals	Formula	Source	Molecular Weight (g mol^{-1})
Ammonium carbonate	$CH_6N_2O_2 \cdot CH_5NO_3$	Merck	157.13
Ammonium meta-vanadate	NH_4VO_3	Riedel-de Haën	116.98
Ammonium perrhenate	NH_4ReO_4	Sigma-Aldrich	268.24
Cerium (III) nitrate hexahydrate	$Ce(NO_3)_3 \cdot 6H_2O$	Sigma-Aldrich	434.23
Oxalic acid dihydrate	$C_2H_2O_4 \cdot 2H_2O$	Alfa Aesar	126.07
Sodium carbonate	Na_2CO_3	Merck	105.99
Tetrachloroauric (III) acid trihydrate	$AuCl_4H \cdot 3H_2O$	Merck	393.83

3.1.2. Gases and Liquids

The specifications and application areas of the liquids and gases used in this study are listed in Table 3.2. and Table 3.3, respectively.

Table 3.2. Specification and application of the liquid used.

Liquid	Specification	Application
Water	De-ionized	Aqueous solutions, Reactant

Table 3.3. Specifications and application area of the gases used.

Gas	Specification	Supplier	Application
Argon	99.998 %	Linde	Inert, GC Carrier Gas
Carbon dioxide	99.995 %	BOS	Reactant, GC calibration
Carbon monoxide	99.999 %	BOS	Reactant, GC calibration
Dry air	99.998 %	Linde	GC 6-way pneumatic valve
Hydrogen	99.990 %	BOS	Reactant, Reduction, GC calibration
Methane	99.500 %	BOS	GC Calibration

3.2. Experimental Systems

There are three main groups of experimental systems used in this study:

(i) Catalyst Preparation Systems: These are the systems used to prepare the support and to carry out impregnation and deposition precipitation steps of catalyst preparation.

(ii) Catalyst Characterization Systems: These systems were used to analyze the structural properties of the catalyst samples.

(iii) Catalytic Reaction System: This catalytic reaction system was used for determining the catalytic activity, selectivity and stability. The continuous flow microreactor system consists of a feed section including mass flow controllers, HPLC pump and a mixing zone; a reaction section including a temperature controlled oven, and an analysis section consisting of a gas chromatograph that is connected on-line to the microreactor flow system.

3.2.1. Catalyst Preparation Systems

The impregnation system (Figure 3.1.) consists of a Retsch UR1 ultrasonic mixer, a vacuum pump, a büchner flask and a MasterFlex computerized-drive peristaltic pump. The system used for deposition precipitation method (Figure 3.2.) includes a Julabo water bath, a 400 ml beaker, a Heidolph impeller and a Mettler Toledo pH-meter.

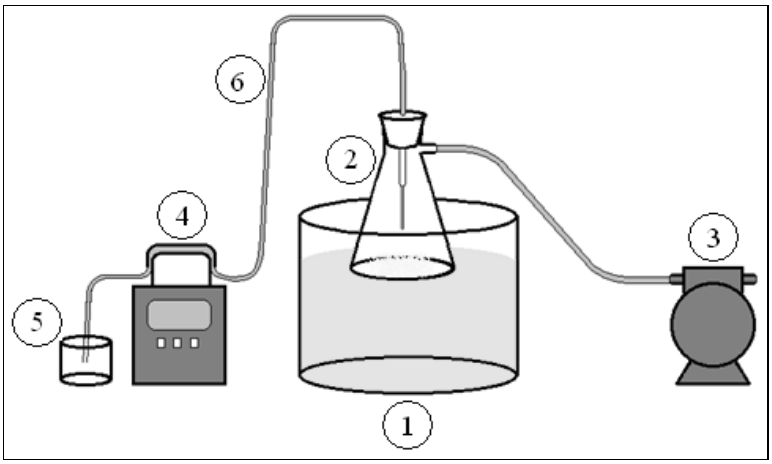

Figure 3.1. Schematic diagram of the impregnation system
(1. Ultrasonic mixer, 2. Büchner flask, 3. Vacuum pump, 4. Peristaltic pump, 5. Precursor solution beaker, 6. Silicone tubing).

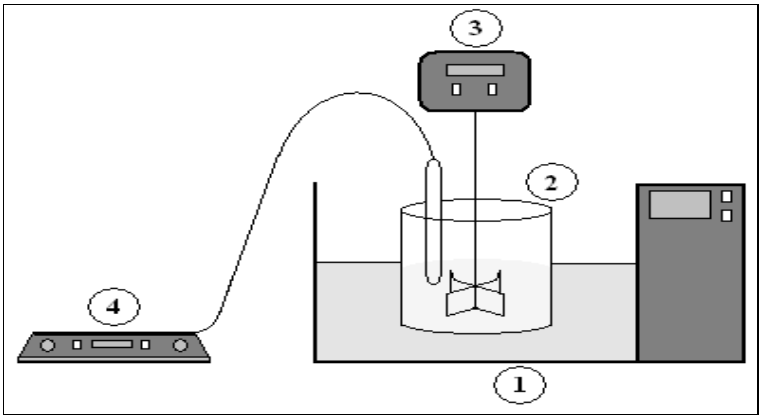

Figure 3.2. Schematic diagram of the deposition precipitation system
(1. Water bath, 2. Beaker, 3. Impeller, 4. pH-meter).

3.2.2. Catalyst Characterization Systems

3.2.2.1. Scanning Electron Microscopy and Energy Dispersive X-Ray (SEM-EDX). Micrograph of the freshly reduced and used samples (Au-Re-V/CeO_2 catalyst samples with different V loadings) after reaction were characterized by SEM and SEM-EDX (Energy Dispersive X-Ray) to analyze their microstructure and metal dispersion, and to observe morphology. The tests were conducted in a Philips XL 30 ESEM-FEG system, having a maximum resolution of 2 nm. The experiments were performed at the Advanced Technologies Research and Development Center of Boğaziçi University.

3.2.2.2. X-ray Photoelectron Spectroscopy (XPS). The extent of electronic interaction between metal components of the freshly reduced catalyst samples was examined through determination the amounts of metallic phases by X-ray photoelectron spectroscopy (XPS) using Thermo Scientific K-Alpha X-ray Photoeleectron Spectrometer. All binding energies were referenced to the C 1s line. For data analysis, the peak intensities were estimated by calculating the integral of each peak, after substraction of the S-shaped Shirley-type background, and by fitting the curve to a combination of Lorentzian (30%) and Gaussian (70%) lines. The analyses were performed at the Advanced Technologies Research and Development Center of Bogazici University.

3.2.2.3. X-Ray Diffraction (XRD). In order to identify the crystalline phases of the catalyst samples and calculating their particle sizes, a Rigaku D/MAX-Ultima+/PC X-ray diffraction equipment having an X-ray generator with Cu target and scan speed of 2°/min was used. The experiments were performed at the Advanced Technologies Research and Development Center of Bogazici University.

3.2.2.4. Raman Spectroscopy. The extents of V–O–Ce bond formation on the catalysts and possible coke formations on spent catalysts were examined with Raman spectroscopy. Raman spectra of the freshly reduced and spent catalyts were obtained by using a Renishaw inVia Raman microscope with the 514 nm 20 mW Ar^+ laser as the excitation source, with 2mW laser intensity, 10 s acquisition time and a total of 5 accumlation per spectrum. The

analyses were performed at the Advanced Technologies Research and Development Center of Bogazici University.

3.2.3. Catalytic Reaction System for WGS Reaction

The catalytic reaction system was designed and constructed in the Catalysis and Reaction Engineering Laboratory of Chemical Engineering Department, Boğaziçi University, and involves feed, reaction and product analysis sections as shown in Figure 3.3.

Feed preparation section consists of mass flow control systems (MFC), an HPLC pump, 1/4", 1/8" and 1/16" stainless steel tubes and fittings for feeding liquid water and gaseous species, i.e. hydrogen, argon, carbon dioxide and carbon monoxide. The reactant gases were supplied by pressurized gas cylinders at the pressure of 2.5 bar. Water was fed to the system with an Agilent Technologies 1200 series HPLC pump while the flow rates of the gases were controlled by Brooks Instrument mass flow controllers. The set of flow rate values were adjusted by the Brooks Instrument 0154 series control box. On-off valves were placed in front of the mass flow controllers to protect them from possible back-pressure fluctuations. Each gas was fed from its independent line, in order to adjust desired feed composition and evaluate the flow of individual species.

The liquid water was introduced into the reaction system at constant flow rates by using an Agilent 1200 series HPLC pump. The 1/16" stainless steel tubing, through which water was allowed to flow and the line going to reactor after the on-off valve, including the reactant mixing zone (mixer/evaporator), were kept about at 140 °C using a 104 W Cole-Parmer heating tape and ceramic wool isolations to provide evaporation and mixing. The temperature level of the mixer/evaporator line was controlled by a Shimaden SR91 programmable temperature controller connected to a K-type fiberglass coated thermocouple.

The reactants, metered and mixed in the feed section, were allowed to flow through the reaction section. This section was composed of a 50 cm × 20 cm × 20 cm furnace, whose temperature was controlled by ±0.1 K through using a Shimaden FP23 programmable temperature controller connected to a K-type sheathed thermocouple. A down-flow 71 cm long ¼” OD stainless steel tubular microreactor was placed inside the furnace. Silane treated

glass wool was placed to the center of the reactor in order to hold the catalyst. Ceramic wool insulations were placed in top and bottom ends of the reactor furnace to prevent heat loss from the furnace. The steam in the product flow is removed at the reactor exit by a cold trap consisting of two condensers connected in series which are placed inside an ice-water bath.

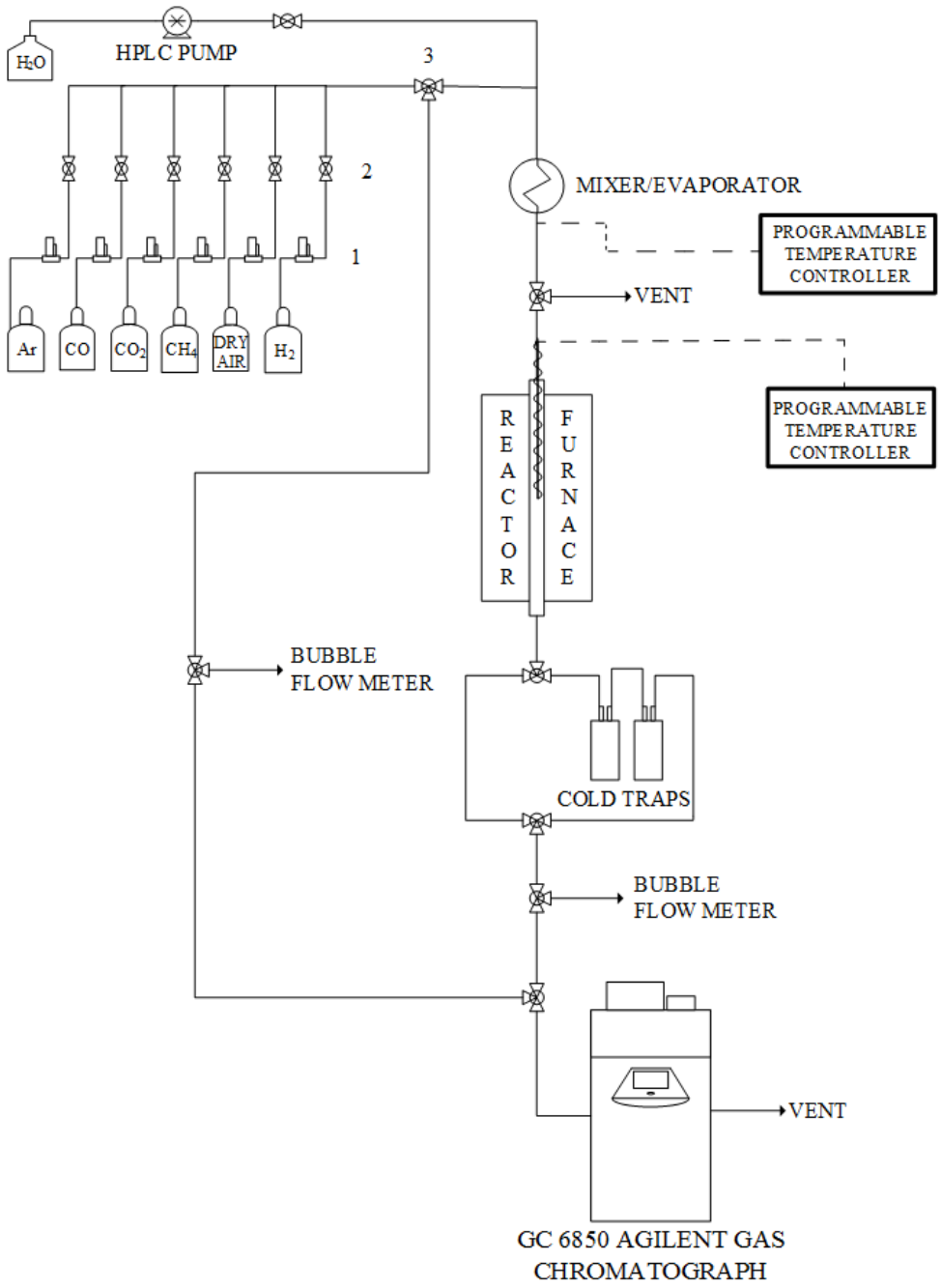

Figure 3.3. Schematic diagram of the microreactor flow system
(1. Mass flow controller, 2. On-off valve, 3. Three-way valve, 4. Mixing zone).

3.2.4. Product Analysis System for WGS reaction

An Agilent Technologies 6850 gas chromatograph equipped with Hayesep D column, and a Thermal Conductivity Detector (TCD) was used to detect feed and dry product streams. The data used for reporting the catalyst performance were hourly time-on-stream (TOS) data. Analysis conditions are given below in Table 3.4.

Table 3.4. Reactant and product gas analysis conditions.

GC Specifications	**Agilent Technologies 6850**
Detector type	TCD
Column temperature, °C	40
Inlet temperature, °C	100
Detector temperature, °C	150
Carrier gas	Argon
Carrier gas flow rate, ml/min	15
Column packing material	Hayesep D
Column tubing material	Stainless steel
Column length & ID	3m x 3 mm
Sample loop	1 ml

Prior to the experiments, the gas chromatograph was calibrated by injecting known values of the gases to be analyzed under the conditions given in Table 3.4. By using this procedure, volume versus peak area curves were obtained for each gas and the corresponding calibration factors were determined by linear regression (Çağlayan, 2011).

3.3. Catalyst Preparation and Pretreatment Procedures

Ceria support was prepared from cerium (III) nitrate hexahydrate precursor, by homogeneous precipitation with sodium carbonate being the precipitation agent. The precipitation agent is dissolved in water and added to the cerium-precursor containing solution which was kept at 60 °C in a water bath. The forming suspension was continuously strirred with an impellar at a rate of 200 RPM. The pH of the solution was monitored with a

pH meter and addition of sodium carbonate continued until pH reached to 8. The obtained suspension was then allowed to age for an hour in a water bath at 60 °C under controlled temperature. A thoroughly stirred mixture was then filtered under vacuum by using Watman filter paper and washed with deionized water, and then dried overnight at 115 °C and calcined for 4 hours at 400 °C (Çağlayan, 2011).

V addition to CeO_2 support was conducted via incipient to wetness impregnation method in the system described in Figure 3.1 by using aqueous solution of ammonium meta-vanadate and oxalic acid dihydrate, where the latter was used to increase solubility of ammonium meta-vanadate. The CeO_2 support was placed in a Büchner flask and kept under vacuum during the process. The support was mixed ultrasonically for 30 minutes before impregnating the aqueous solution. The precursor solution containing the mixture of ammounium meta-vanadate and oxalic acid at 1:1.5 molar ratio was impregnated on the support by using Masterlex computerized-drive peristaltic pump at a rate of 0.5 ml/min. The resulting slurry was mixed ultrasonically in order to obtain uniform distribution of the precursor solution on the ceria support. After 1.5 h, the resulting slurry was dried overnight at 115 °C and calcined for 2 hours at 400 °C at a muffle furnace.

Re addition to V impregrated CeO_2 support was conducted via incipient to wetness impregnation method in the system described in Figure 3.1 by using aqueous solution of ammonium perrhenate. The V impregrated CeO_2 support was placed in a Büchner flask and kept under vacuum during the process. The support was mixed ultrasonically for 30 minutes before impregnating the aqueous solution. The precursor solution was impregnated on the support by using Masterlex computerized-drive peristaltic pump at a rate of 0.5 ml/min. The resulting slurry was mixed ultrasonically in order to obtain uniform distribution of the precursor solution on the ceria support. After 1.5 h, the resulting slurry was dried overnight at 115 °C (Çağlayan, 2011).

Deposition precipitation technique was used to obtain highly dispersed Au particles on the V and Re impregnated CeO_2 supports. The V and Re impregnated support was placed in a beaker along with deionized water at a pH of 8.0-8.5 by adding aqueous solution of ammonium carbonate. Tetrachloro auric (IV) acid was dissolved in deionized water and added dropwise in 40-45 minutes under continuous stirring that was provided by the

ultrasound mixer. The resulting precipitate was aged for 1 h, filtered and washed with deionized water at 65 °C. The filtrate was allowed to dry overnight at 75 °C under vacuum and calcined at air in a muffle furnace at 400 °C for 4 h (Çağlayan, 2011).

All catalysts tested in this study were prepared in the sequence mentioned above. The list of Au, Re and V loadings on CeO_2 supports are shown in Table 3.5. Prior to the reaction tests, the catalyst samples were reduced *in situ* under 5% hydrogen and 95% nitrogen flow feed for 1 h at 200 °C at a flow rate of 100 ml/min. The temperature of the furnace is increased at a rate of 7.5 °C/min.

Table 3.5. List of Au-Re-V/CeO_2 trimetallic catalysts.

Catalyst Name	Au wt%	Re wt%	V wt%
1Au-0.5Re-3V/CeO_2	1	0.5	3
1Au-0.5Re-1V/CeO_2	1	0.5	1
1Au-0.5Re-0.5V/CeO_2	1	0.5	0.5

3.4. Performance Tests

The WGS performance of Au-Re-V/CeO_2 catalysts given in Table 3.5 was investigated at 200, 250, 300, 350 and 400 °C for two ideal and two realistic feed compositions. The feed conditions for realistic and ideal cases are given in Tables 3.6 and 3.7, respectively. Each experiment was conducted over 75 mg freshly reduced catalyst with 120,000 ml g_{cat}^{-1} h^{-1} GHSV.

Table 3.6. Ideal feed compositions used in the current study.

Feed	H_2O/CO	CO%	H_2O %	Ar %
Ideal #1	5.0	3.0	15.0	82.0
Ideal #2	2.0	3.0	6.0	91.0

Table 3.7. Realistic feed compositions used in the current study.

Feed	H_2O/CO	CO%	H_2O %	H_2 %	CO_2 %	Ar %
Realistic #1	6.7	4.9	32.7	30.0	10.4	22.0
Realistic #2	16.2	2.1	34.1	23.7	12.3	27.8

After reduction, the catalyst bed heated to the reaction temperature, and Ar gas trapped in the reactor while the reactants with specified compositions were bypassed for 1.5 hour in order to obtain steady state gas composition. A list of the performed experiments is given in Table 3.8.

Table 3.8. Summary of the performed experiments.

Experiment Number	Catalyst	Feed	Temperature (°C)
1	1Au-0.5Re-1V/CeO_2	Ideal 1	400
2	1Au-0.5Re-1V/CeO_2	Ideal 1	350
3	1Au-0.5Re-1V/CeO_2	Ideal 1	300
4	1Au-0.5Re-1V/CeO_2	Ideal 1	250
5	1Au-0.5Re-1V/CeO_2	Ideal 1	200
6	1Au-0.5Re-1V/CeO_2	Ideal 2	400
7	1Au-0.5Re-1V/CeO_2	Ideal 2	350
8	1Au-0.5Re-1V/CeO_2	Ideal 2	300
9	1Au-0.5Re-1V/CeO_2	Ideal 2	250
10	1Au-0.5Re-1V/CeO_2	Ideal 2	200
11	1Au-0.5Re-1V/CeO_2	Realistic 1	400
12	1Au-0.5Re-1V/CeO_2	Realistic 1	350
13	1Au-0.5Re-1V/CeO_2	Realistic 1	300
14	1Au-0.5Re-1V/CeO_2	Realistic 2	400
15	1Au-0.5Re-1V/CeO_2	Realistic 2	350
16	1Au-0.5Re-1V/CeO_2	Realistic 2	300
17	1Au-0.5Re-3V/CeO_2	Ideal 1	400
18	1Au-0.5Re-3V/CeO_2	Ideal 1	350

Table 3.8. Summary of the performed experiments (cont'd).

Experiment Number	Catalyst	Feed	Temperature (°C)
19	1Au-0.5Re-0.5V/CeO_2	Ideal 1	400
20	1Au-0.5Re-0.5V/CeO_2	Ideal 1	350
21	1Au-0.5Re-0.5V/CeO_2	Ideal 1	300
22	1Au-0.5Re-0.5V/CeO_2	Ideal 1	250
23	1Au-0.5Re-0.5V/CeO_2	Ideal 2	400
24	1Au-0.5Re-0.5V/CeO_2	Ideal 2	350
25	1Au-0.5Re-0.5V/CeO_2	Ideal 2	300
26	1Au-0.5Re-0.5V/CeO_2	Ideal 2	250
27	1Au-0.5Re-0.5V/CeO_2	Realistic 1	400
28	1Au-0.5Re-0.5V/CeO_2	Realistic 1	350
29	1Au-0.5Re-0.5V/CeO_2	Realistic 1	300
30	1Au-0.5Re-0.5V/CeO_2	Realistic 2	400
31	1Au-0.5Re-0.5V/CeO_2	Realistic 2	350
32	1Au-0.5Re-0.5V/CeO_2	Realistic 2	300
33	1Au-0.5Re/CeO_2	Ideal 1	400

TOS starts with the first contact between reactant gases and catalyst bed. Product analyses were first done 30 minutes after contact. Then at every hour end (after contact) the product was analyzed. Feed analyses were done at the end of product analyses. A total of seven product analyses and three feed analyses were made during each performance tests.

4. RESULTS AND DISCUSSIONS

Results and discussions are presented in two sections. First section consists of the WGS performance test results. In the studies, effects of reaction temperature, feed composition and catalyst composition on the WGS performance were investigated.

In the second section, the results of the characterization analyses are reported. Characterization analyses are powerful tools to investigate physical and chemical properties of a catalyst. This chapter contains the SEM-EDX, XPS, XRD, and Raman spectroscopy analyses for all trimetallic Au-Re-V/CeO_2 catalysts. The results of the characterization analyses are used to explain the performance test results.

4.1. WGS Performance Tests

In the performance tests, WGS activity and stability characteristics of the catalysts listed in Table 3.8 were investigated. Catalytic activity is reported as CO conversion for ideal feeds and CO conversion and amount of net H_2 produced for realistic feeds. In comparing the activities of catalyst samples, activity values at the end of 1 h TOS are used (Figures 4.1 to 4.7). Blank tests were previously conducted for stainless steel reactors and CeO_2 support by Çağlayan in 2011; the results confirmed both the system and the support have no WGS activity (Çağlayan, 2011). TOS activity and stability data of all performance tests are given in Appendix A.

Calculation procedures for CO conversion and amount of net H_2 produced are given in Equations 4.1 and 4.2:

$$\text{CO conversion (\%)} = \left[\frac{n_{CO,in} - n_{CO,out}}{n_{CO,in}}\right] 100 \tag{4.1}$$

$$\text{Net } H_2 \text{ production (\%)} = \left[\frac{n_{H_2,out} - n_{H_2,in}}{n_{H_2,in}}\right] 100 \tag{4.2}$$

where number of moles in both feed and product streams are calculated by using Equation 4.3:

$$n_i\ (\mu mol\ s^{-1}) = \frac{P\ V_{i,gas}}{R\ T} \tag{4.3}$$

where P is the atmospheric pressure, $V_{i,gas}$ is the volumetric flow rate of the gas, R is the universal gas constant, and T is the absolute temperature.

Activity loss is a measure of stability of the catalyst. It is usually reported as the percent loss of initial activity. Equation 4.4 shows how activity loss is calculated:

$$\text{Activity loss } (\%) = \left[\frac{(\text{CO conversion})_{0.5h} - (\text{CO conversion})_{6h}}{(\text{CO conversion})_{0.5h}}\right] 100 \tag{4.4}$$

4.1.1. Ideal Feed Tests

The tests were conducted under atmospheric pressure and at temperatures of 200, 250, 300, 350, and 400 ºC. GHSV was fixed at 120,000 ml g_{cat}^{-1} h^{-1} for all tests. The specifications of two ideal feeds used are given in Table 3.6.

Figures 4.1 and 4.2 present temperature dependence of catalytic activity of the trimetallic Au-Re-V/CeO_2 catalysts under the flow of ideal feed #1 (H_2O/CO = 5) and ideal feed #2 (H_2O/CO = 2), respectively. Figures also include the equilibrium conversion of CO that was determined by thermodynamics. Both figures indicate superior activity of 1Au-0.5Re-0.5V/CeO_2 over other trimetallic catalysts with higher V-loadings. 1Au-0.5Re-1V/CeO_2 showed significantly higher activity compared to 1Au-0.5Re-3V/CeO_2.

The WGS activity increased with increasing reaction temperature for all catalysts tested under the flow of ideal feed #1. It should be noted that 1Au-0.5Re-1V/CeO_2 showed only small increase in activity at temperatures greater than 300 ºC; whereas activity of 1Au-

0.5Re-0.5V/CeO_2 increased dramatically at 400 ºC after stagnating between 300 and 350 ºC. The highest activity achieved by 1Au-0.5Re-0.5V/CeO_2 was 88.4% CO conversion as opposed to 98.0% equilibrium conversion at 400 ºC. 1Au-0.5Re-1V/CeO_2 also showed its highest activity at 400 ºC with 49.2% conversion. CO conversion decreased far below equilibrium conversion with decreasing temperature, as evidenced by Figures 4.1 and 4.2.

Note that there are only two tests performed for 1Au-0.5Re-3V/CeO_2 catalyst. Due to poor performance of 1Au-0.5Re-3V/CeO_2 at 350 and 400 ºC, no further performance test for this catalyst was done. The highest activity observed over 3 wt% loaded sample was 3.4% at 400 ºC. A reason for bad performance of the catalyst might be the large size Au-Re clusters formed on the support surface. Au is reported to be active only when the particle size is small such as 4.5-9 nm (LeValley *et al.*, 2014).

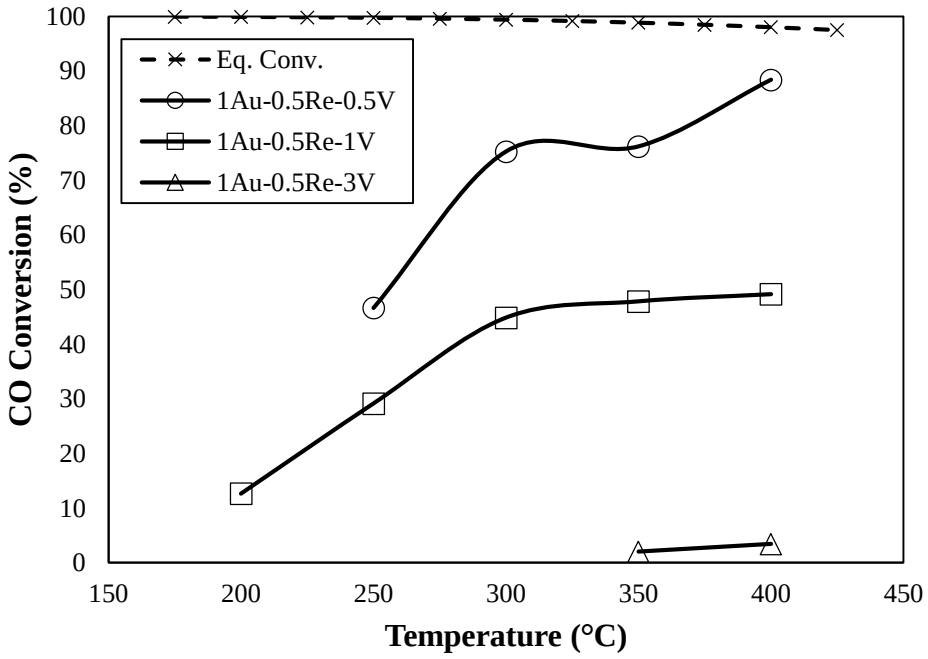

Figure 4.1. Temperature dependence of the catalytic activity for ideal feed # 1 (3 % CO, 15 % H_2O, 82 % Ar; H_2O/CO = 5).

As evidenced by Figure 4.2 1Au-0.5Re-0.5V/CeO_2 still prevailed as the more active catalyst at low H_2O/CO feed ratio. Unlike the high H_2O/CO feed ratio case, this time the activities of both catalysts peaked at mid temperatures and began to decrease with further temperature increase. CO conversion of 1Au-0.5Re-0.5V/CeO_2 increased drastically as

temperature increased from 250 to 300 ºC. At 300 ºC, 74.9% CO conversion was achieved as opposed to 97.7% equilibrium conversion limit. After 300 ºC, activity gradually dropped with increasing temperature. 1Au-0.5Re-1V/CeO_2 showed a similar behavior, although maximum activity was observed at 350 ºC with 43.6% CO conversion.

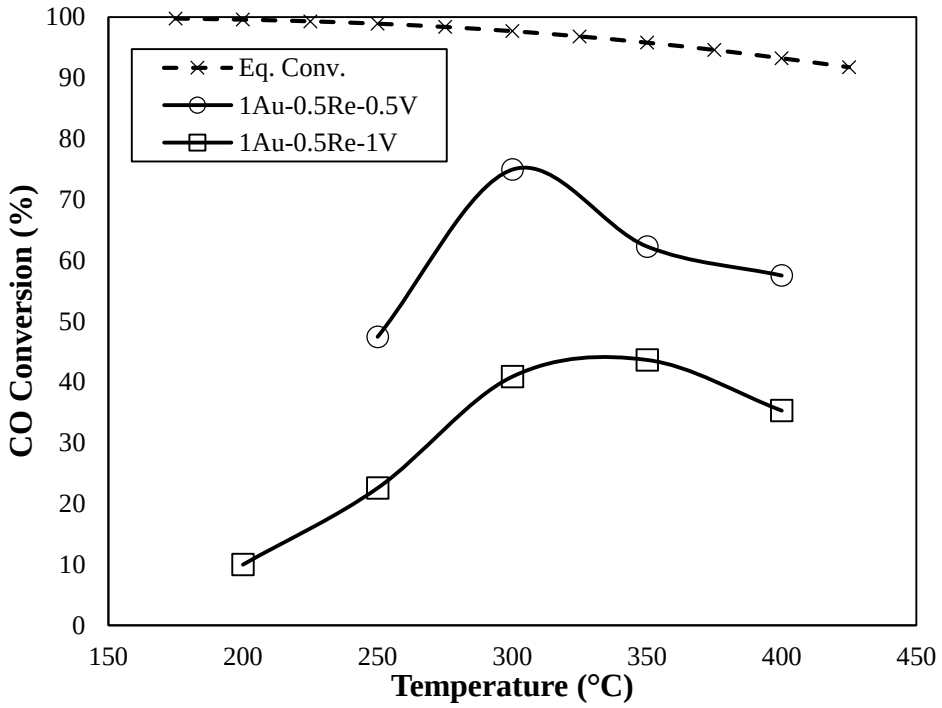

Figure 4.2. Temperature dependence of the catalytic activity for ideal feed # 2 (3 % CO, 6 % H_2O, 91 % Ar; H_2O/CO = 2).

A comparison of catalytic activities obtained under the flow of ideal feeds #1 and #2 over 1Au-0.5Re-1V/CeO_2 is made in Figure 4.3. CO conversion increased from 200 to 300 ºC for both ideal feeds. Though there were slight increases, CO conversion values did not change significantly between 300 and 350 ºC for both feeds; however, the activity significantly dropped for low H_2O/CO feed ratio at 400 ºC. CO conversion has its maximum at 400 ºC over 1Au-0.5Re-1V/CeO_2 catalyst at high H_2O/CO feed ratio. Even the highest CO conversion obtained over this catalyst is significantly lower than the equilibrium conversion (see Figures 4.1 and 4.2).

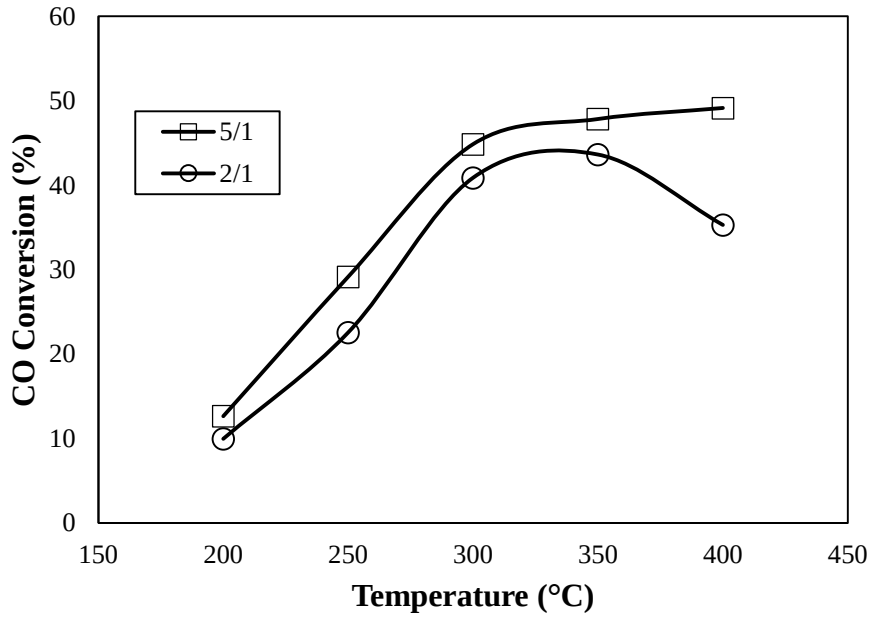

Figure 4.3. Effect of H_2O/CO feed ratio on the catalytic activity of 1Au-0.5Re-1V/CeO_2.

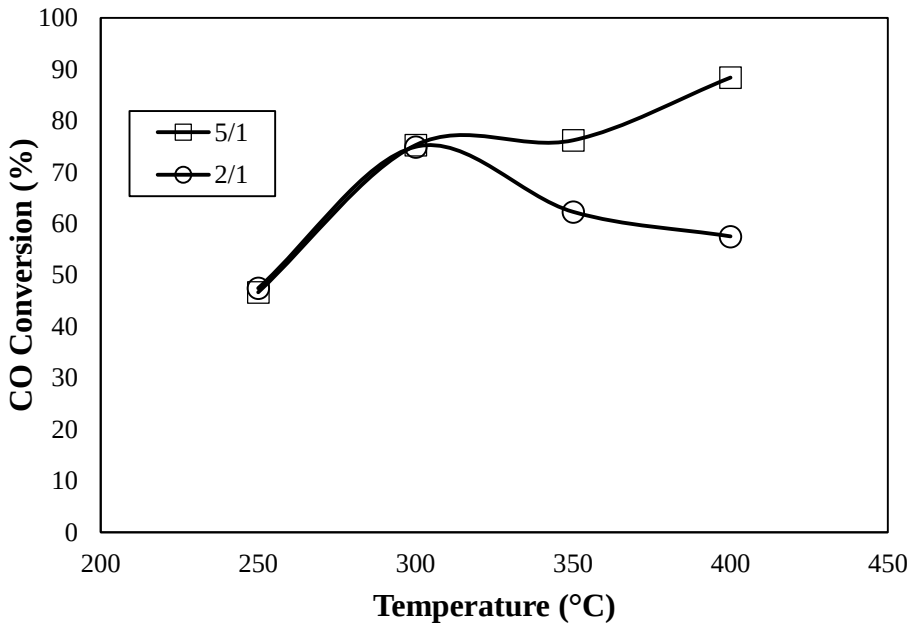

Figure 4.4. Effect of H_2O/CO feed ratio on the catalytic activity of 1Au-0.5Re-0.5V/CeO_2.

Figure 4.4 shows the comparison of catalytic activities obtained under the flow of ideal feeds #1 and #2 over 1Au-0.5Re-0.5V/CeO_2. Note that performance tests at 200 ºC are skipped for this catalyst due the low activities previously observed over 1Au-0.5Re-1V/CeO_2 at this temperature.

A comparative analysis of activity trends of 1Au-0.5Re-0.5V/CeO_2 sample for feeds with H_2O/CO ratio of 5 and 2 (Figure 4.4) reveals that the activity increases with temperature up to 300 ºC for both feeds. On the other hand, though the activity makes a plateau at 300-350 ºC interval and significanty increases with a further increase in temperature to 400 ºC for high H_2O-content feed, there observed a continuous decrease in activity with temperature above 300 ºC for low H_2O-content feed. The reason of the decrease in activity may be the increase in the rate of reverse WGS activity, which may become significant when H_2O/CO ratio of the feed is low.

Figure 4.5 shows a comparison of WGS performance of three Au-Re-V/CeO_2 catalysts with different V-loadings under the flow of ideal feed #1 at 400 ºC. Note that the activity and stability of bimetallic 1Au-0.5Re/CeO_2 catalyst was previously investigated by Çağlayan (Çağlayan, 2011). The reaction was done at 400 ºC and with ideal feed #1. The CO conversion profiles suggest that V addition gradually decreases the catalytic activity of Au-Re system. While 0.5 wt% V addition resulted in comparable activity and stability to previously tested 1Au-0.5Re/CeO_2, as the loading of V was increased to 1 wt%, the CO conversion was nearly halved. Further increase of V loading to 3 wt% diminished CO conversion to values around 3-4 % conversion.

In TOS tests, the activities of all three catalysts decreased. The activity losses in 6 h TOS tests were found as 37 (Çağlayan, 2011), 19.9, and 27.7 % for 1Au-0.5Re/CeO_2, 1Au-0.5Re-0.5V/CeO_2, and 1Au-0.5Re-1V/CeO_2, respectively.

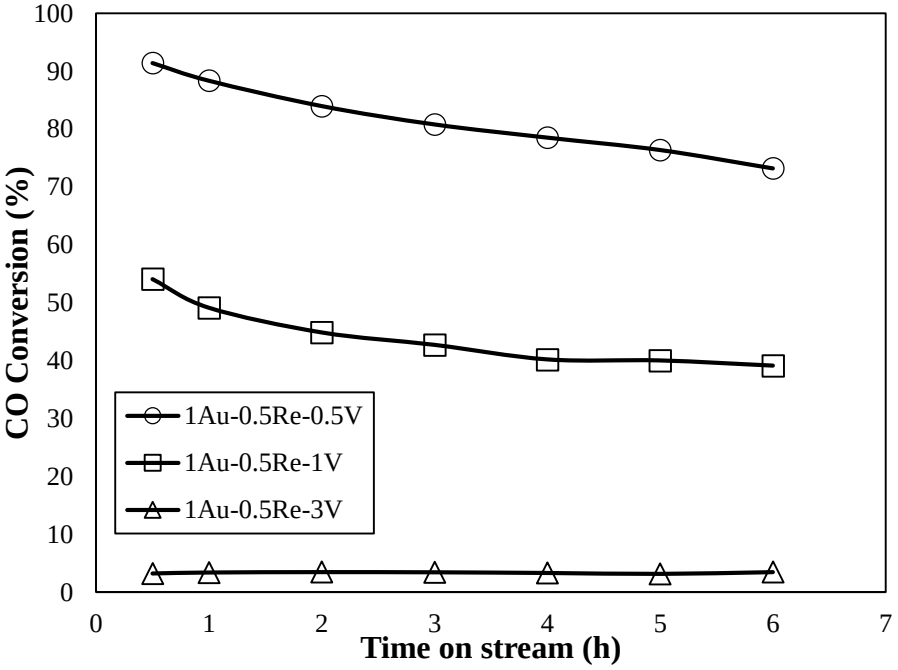

Figure 4.5. Effect of V-loading on the activity for ideal feed #1 at 400 ºC (3 % CO, 15 % H_2O, 82 % Ar; H_2O/CO = 5).

The activity losses were recorded for all ideal feed experiments for trimetallic Au-Re-V catalysts. 1Au-0.5Re-0.5V/CeO_2 catalyst experienced activity losses ca. 20 % at 6 h TOS with both feeds in temperature range of 250-400 ºC. Higher activity losses were observed for 1Au-0.5Re-1V/CeO_2. There seemed no correlation between reaction temperature and catalyst stability for 1Au-0.5Re-0.5V/CeO_2 when both ideal feeds were considered. On the other hand, the activity loss appeared to be increased for 1Au-0.5Re-1V/CeO_2 as the reaction temperature was decreased. The activity loss results showed that 1Au-0.5Re-0.5V/CeO_2 catalyst was more stable compared to 1Au-0.5Re-1V/CeO_2 under all reaction conditions. The results indicated that 0.5 wt% V promotion limits the activity loss, which was 37 % over 1Au-0.5Re/CeO_2 catalyst at 350 ºC (Çağlayan, 2011).

4.1.2. Realistic Feed Tests

Performance test results for two realistic feeds specified in Table 3.7 are given and discussed in this section. Realistic feeds were chosen to simulate typical reformer effluent streams. The tests were conducted under atmospheric pressure and at temperatures of 300,

350, and 400 ºC. During the tests, GHSV was kept at 120,000 ml g_{cat}^{-1} h^{-1}. Methane formation was not detected at any reaction condition, showing the Au-Re-V system indeed suppressed secondary methanation activity.

Figures 4.6a and 4.6b display the CO conversions and the amount of net H_2 produced for realistic feed #1 (H_2O/CO = 6.7), respectively. Similar to what was observed during performance tests with ideal feed, 1Au-0.5Re-0.5V/CeO_2 catalyst had higher performance than that of 1Au-0.5Re-1V/CeO_2 at any temperature.

Activity of 1Au-0.5Re-1V/CeO_2 increased as the temperature increased; the highest CO conversion obtained was 9.3% at 400 ºC. This resulted in production of 4.3 % additional H_2 to 30.2 µmol/s H_2 already present in the feed. As the wt% of V was decreased to 0.5 wt% the catalytic activity was improved. For 1Au-0.5Re-0.5V/CeO_2, an increase in CO conversion from 26.2 to 29.9% accompanied by an increase in net H_2 production from 8.5 to 10.0 %, was observed when temperature was changed from 300 to 350 ºC. Increasing temperature further to 400 ºC led to drop in both CO conversion and additional H_2 production by 21.2 and 6.3 %, respectively. For all cases, the conversion obtained was far below the equilibrium conversion.

The most succesful catalyst of this study, 1Au-0.5Re-0.5V/CeO_2, showed less activity compared to Çağlayan's 1Au-0.5Re/CeO_2. 1Au-0.5Re/CeO_2 yielded 43 and 38% CO conversions at 300 and 350 ºC, respectively. However, additional H_2 production of 1Au-0.5Re-0.5V/CeO_2 was superior both at 300 and 350 ºC (Çağlayan, 2011).

Activity losses are calculated via comparing 0.5 h and 6 h TOS data. Activity loss was found to be strongly dependent on the reaction temperature. Though 1Au-0.5Re-0.5V/CeO_2 catalyst showed relatively higher stability especially at higher temperatures; both catalysts experienced severe deactivation throughout the six hour performance tests. 1Au-0.5Re-0.5V/CeO_2 showed relatively more stable performance at 400 ºC with 49.4 % activity loss; whereas 1Au-0.5Re-1V/CeO_2 experienced 44.8 % activity loss at the same temperature. Activity loss of 1Au-0.5Re-1V/CeO_2 reached to 82.2 % at 300 ºC.

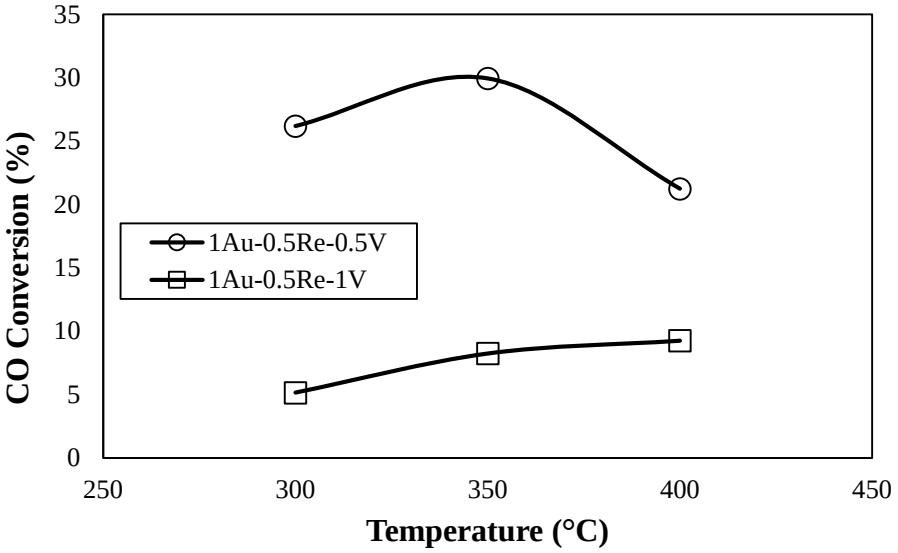

(a)

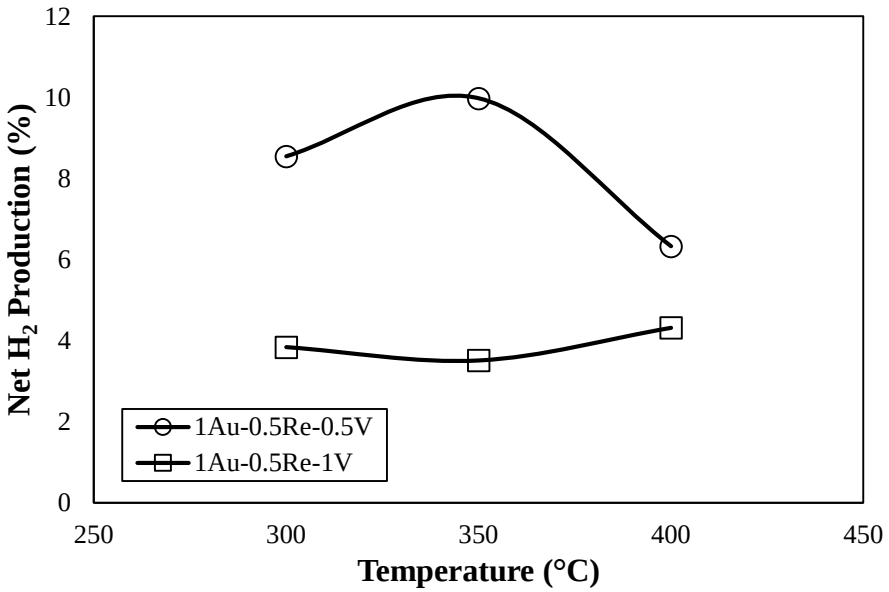

(b)

Figure 4.6. Temperature dependence of (a) catalytic activity and (b) net H_2 production for realistic feed # 1 (4.9 % CO, 32.7 % H_2O, 30.0 % H_2, 10.4 % CO_2, 22.0 % Ar; H_2O/CO = 6.7).

Figures 4.7a and 4.7b display the CO conversions and the amount of net H_2 produced for realistic feed #2 (H_2O/CO = 16.2), respectively. 1Au-0.5Re-0.5V/CeO_2 and 1Au-0.5Re-1V/CeO_2 catalysts have similar activity-temperature relations compared to their performance behaviour with realistic feed #1.

1Au-0.5Re-0.5V/CeO_2 activity peaked at 350 ºC, with 26.6% CO conversion and 6.4 % additional H_2 production to 24.2 µmol/s H_2 coming from the feed. CO conversions drop to 21.6 and 21.9% at 300 and 400 ºC, respectively. 1Au-0.5Re-1V/CeO_2 catalyst showed its highest activity at 400 ºC with 9.5% CO conversion along with 3.7 % additional H_2 production. Results indicated that experimental CO conversion values were far below equilibrium conversion values. Although an evident change in activity with temperature was observed for 1Au-0.5Re-1V/CeO_2, its net H_2 production values seem to be similar for the temperature range tested.

Compared to activity test results of 1Au-0.5Re/CeO_2 for realistic feed #2 (Çağlayan, 2011), 1Au-0.5Re-0.5V/CeO_2 still showed less activity; bimetallic 1Au-0.5Re/CeO_2 gave almost equilibrium level conversions around 86 and 74 % CO conversions at 300 and 350 ºC, respectively (Çağlayan, 2011). On the other hand, an improvement was observed in net H_2 production; Çağlayan found net H_2 production 350 ºC as negative, while 1Au-0.5Re-1V/CeO_2 managed to produce additional H_2.

The relation between H_2O/CO ratio of the feed and activity loss observed at 6h TOS indicated that both catalysts were more stable when realistic feed #2 having high H_2O/CO ratio, 16.2, was used. For the same feed, there is still a slight dependence of activity loss to temperature. Though the activity loss of 0.5 wt% V loaded sample decreases with an increase in temperatures, it makes a peak at 350 ºC over 1 wt% V loaded sample. It should be noted that the activity loss is significant, ca. 50 %, over 0.5 wt% V promoted sample even at 400 ºC under the flow of H_2O-rich realistic feed #2.

Comparative analysis of the performance results obtained under the flow of two realistic feeds show that realistic feed #1 with low H_2O/CO yields higher net H_2 production values. This result can be explained by considering a previous kinetic study on 1Au-0.5 Re/CeO_2 catalyst, where rate orders for CO, H_2O, CO_2, and H_2 were found as 0.75, 2.00, -0.34, and -0.60, respectively (Gökaliler, 2011). For both realistic feeds, H_2O amounts are very similar: 32.7% for realistic feed #1 and 34.1% for realistic feed #2. CO_2 amounts are also similar: 10.4% of realistic feed #1 compared to 12.3% of realistic feed #2. The main difference between two feeds is the amount of CO. Realistic feed #1 contains almost 2.5 times of more CO (4.9%) compared to realistic feed #2 (2.1%), hence WGS rate was limited

for realistic feed #2 as contribution of CO term in kinetics expression is limited due to low CO content of the feed.

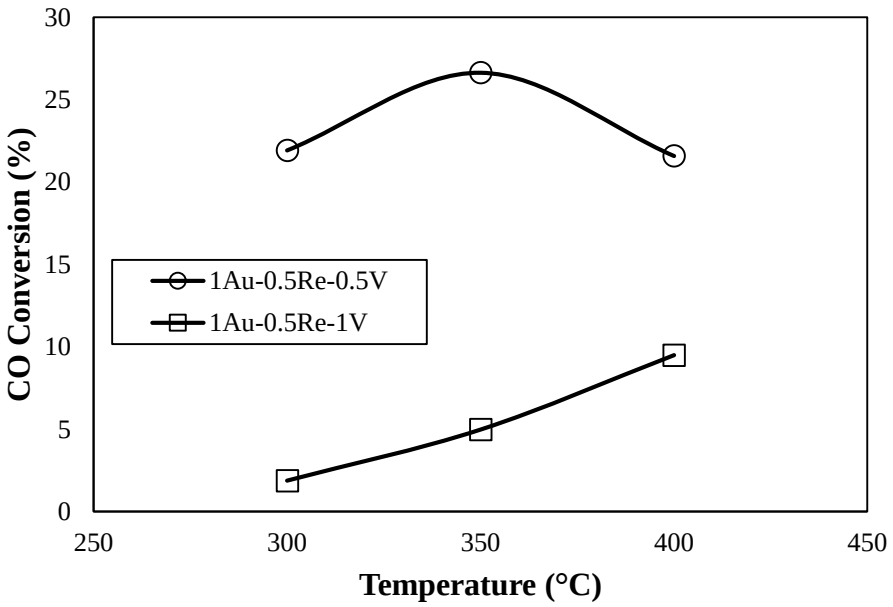

(a)

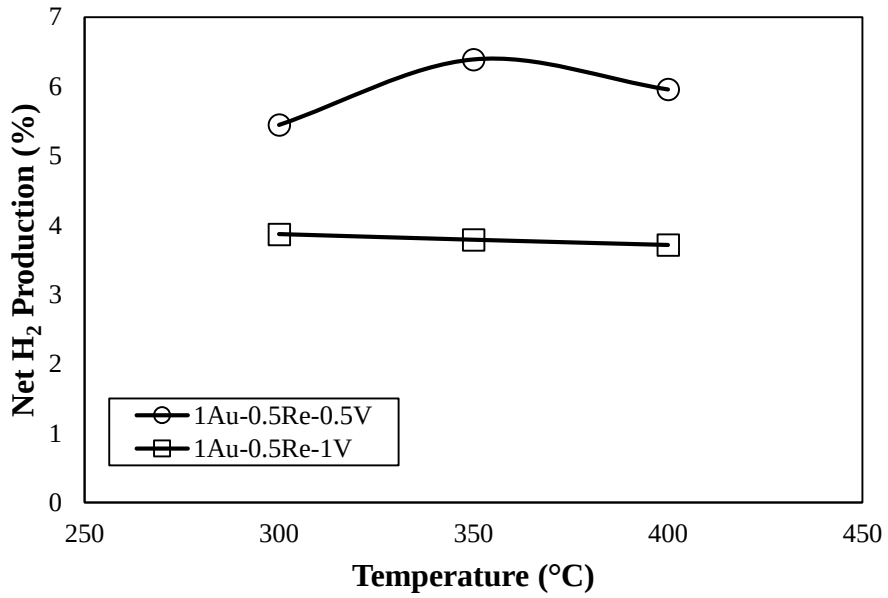

(b)

Figure 4.7. Temperature dependence (a) catalytic activity and (b) net H_2 production for realistic feed # 2 (2.1 % CO, 34.1 % H_2O, 23.7 % H_2, 12.3 % CO_2, 27.8 % Ar; H_2O/CO = 16.2).

4.2. Catalyst Characterization

4.2.1. SEM-EDX

In order to investigate the microstructural properties of the catalyst, scanning electron microscopy (SEM) with energy dispersive X-ray (EDX) analyses were performed.

Freshly reduced and spent Au-Re-V catalysts prepared were characterized by using SEM-EDX to obtain information on their microstructural and metal dispersion properties, and the presence and type of carbon deposit formed on their surface during WGS. Metal mapping studies were performed to understand the dispersion of metals and whether the agglomeration of metals occurs on the support surface during reaction. For reduced and spent catalyst samples, SEM bright area images with 100,000x magnification are given in Figures 4.8 and 4.9, respectively.

Figure 4.8a-c allow comparison of microstructures of freshly reduced Au-Re-V catalysts with different V-loadings. All samples showed the characteristic blossom/petal-like structure of CeO_2 support prepared by homogenous precipitation method (Çağlayan and Aksoylu, 2011). Atomic weights, hence brightness of V- and Ce-atoms are similar; this is the reason why V-atoms on the surface were not distinguishable to secondary electron (SE) or back scattering electron (BSE) detectors. Au- and Re-atoms have larger atomic weights than V or Ce; thus, clusters of Au and Re were expected to be visible. However, no Au- or Re-clusters were seen in Figures 4.8a and 4.8b. EDX and mapping analysis confirm existence of Au- and Re-atoms on the surface; therefore it was suggested that when V-loading is 0.5 and 1 wt%, Au and Re atoms might have migrated into pores of the support and/or had very high dispersion. High dispersion of Au and Re atoms is a plausible explanation considering the deposition precipitation method used for Au addition, which strictly favors small sized Au particles on the support surface.

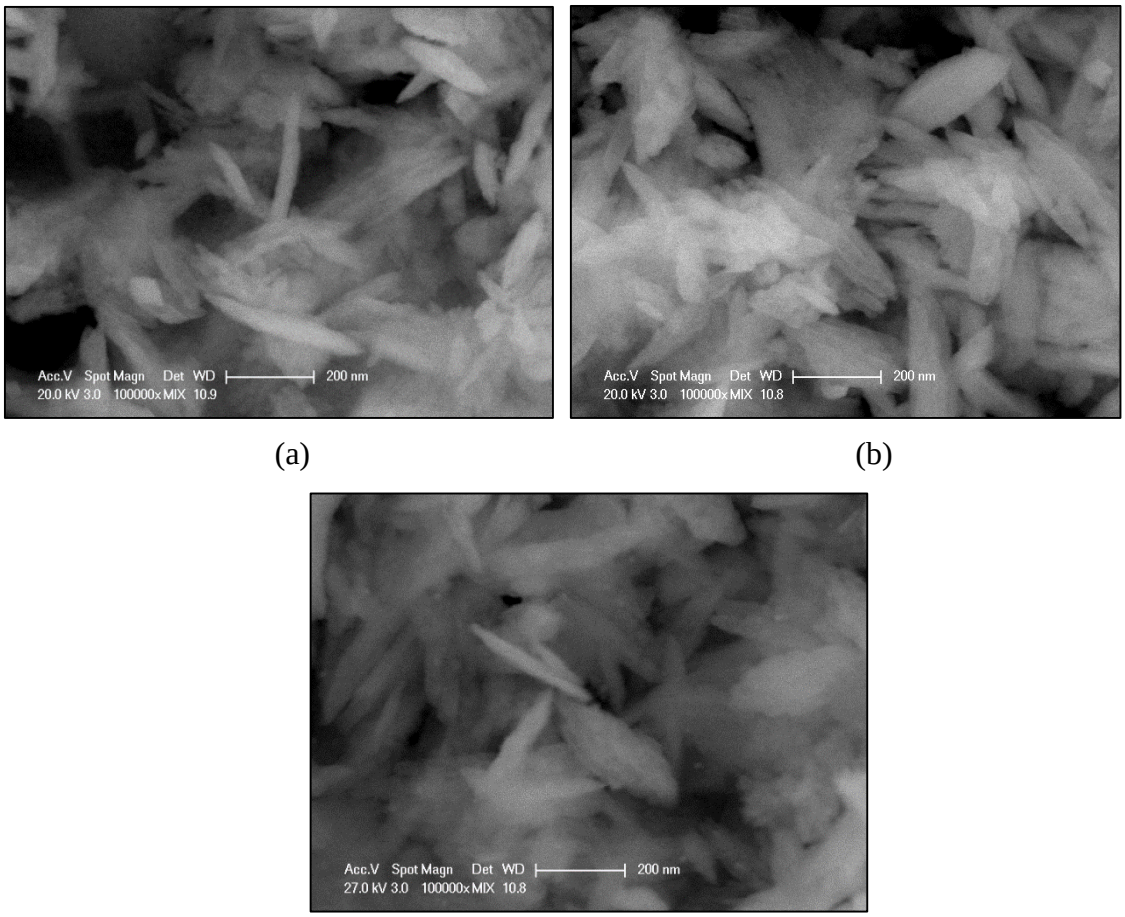

Figure 4.8. SEM bright area images of freshly reduced catalysts (100000x) for (a) 1Au-0.5Re-0.5V/CeO_2, (b) 1Au-0.5Re-1V/CeO_2, and (c) 1Au-0.5Re-3V/CeO_2.

Figure 4.8c showed when V-loading was increased to 3 wt% the microstructural properties became different from those observed for 0.5 and 1 wt% V loaded samples. In SEM image of 1Au-0.5Re-3V/CeO_2, bright areas of approx. 20 nm diameter were seen. Homogeneous distribution of bright areas around the entire catalyst was confirmed by SEM-EDX analyses performed for different regions of the catalyst sample. Owing to high contrast in brightness of support and the spots, it is safe to assume that they are Au and/or Re clusters. CeO_2 is reported to increase dispersion of Au atoms (Esch *et al.*, 2005), whereas VO_x's on the surface might have caused Au and Re atoms to agglomerate.

Performance test results showed that the catalytic activity decreased with the increase in V-loading. The low activity of 1Au-0.5Re-3V/CeO_2 can be explained by the large particle

size of Au and Re atoms, hence low dispersion. It is known that catalytic activity of Au-based catalysts is maximized when Au is very well dispersed and Au-O linkages are exposed to gaseous reactants (Liu *et al.*, 2013-LeValley *et al.*, 2014). Consequently, 3 wt% V loaded sample which has large sized Au clusters in the SEM image, has low activity.

Spent catalyst surfaces were investigated for coke formation and/or agglomeration of metal phases on the support. 1Au-0.5Re-0.5V/CeO_2 tested under both realistic feed compositions at 350 °C were chosen as the spent samples. Both catalysts showed high initial activity but after 6 h their activities were decreased. SEM images were examined to seek out possible reasons of catalyst deactivation. Figures 4.9a and 4.9b showed that there was no significant change in microstructure of the catalyst surfaces after 6 h TOS reaction with feed having high and low H_2O/CO ratios. V atoms were not visible due to low difference in contrast with CeO_2 support. Au and Re metals were also not visible, thus agglomeration of metals were ruled out as possible reason of deactivation.

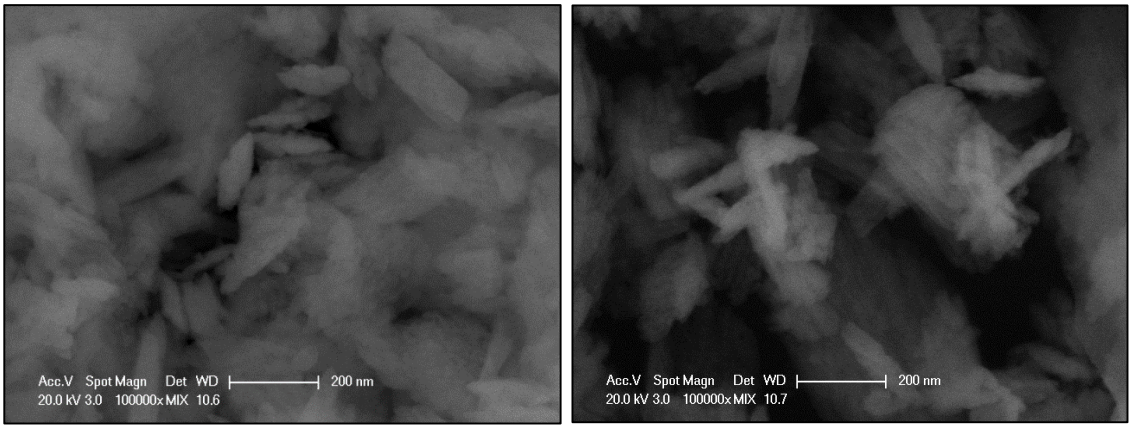

(a) (b)

Figure 4.9. SEM bright area images of spent 1Au-0.5Re-0.5V/CeO_2 catalysts (100000x) for (a) realistic feed #1 and (b) realistic feed #2.

Metal mapping images of 1Au-0.5Re-0.5V/CeO_2 catalyst is shown in Figure 4.10. The mappings of Au, Re, V, and Ce indicated that metal dispersions have good homogeneity over CeO_2 support.

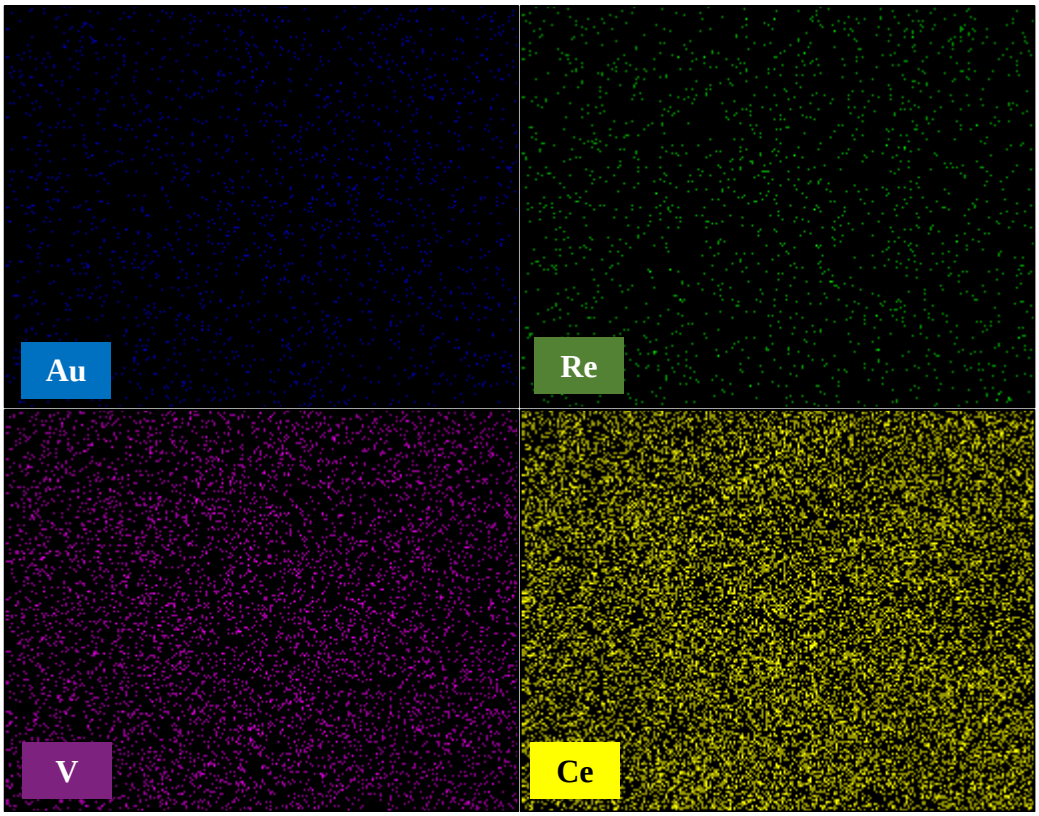

Figure 4.10. Mapping of freshly reduced 1Au-0.5Re-0.5V/CeO_2 catalyst.

Instructor's manual of the Philips XL30 ESEM-FEG/EDAX system stated EDX analysis results are not reliable when the analyzed specimen has constituents with lower than 2 wt% amount. For this reason, loadings of Au and Re have are not given in this section. Thus, the analysis was carried out to confirm the loading of V. However, as K and L energy levels of V-atoms in EDX analysis overlapped with L and K energy levels of Ce- and O-atoms, respectively, EDX analysis was also found inappropriate for this catalyst system.

4.2.2. XPS

Oxidation states and elemental compositions of the atoms on the catalyst surface were examined by X-ray photoelectron spectroscopy (XPS) method. XP spectra of the catalysts show characteristic oxidation states of Ce, O, V, Re, and Au atoms. Since CeO_x and VO_x are known to have redox properties, XPS analysis on both reduced and spent samples provided insight into changes occurred on the catalyst surface during reaction.

The binding energies and corresponding peaks for principal spin-orbit states, Ce $3d_{3/2}$ and Ce $3d_{5/2}$, are shown in Figure 4.11. CeO_x is reported to exhibit unique redox properties. Ce atoms have two oxidation states: Ce^{3+} and Ce^{4+}, in Ce $3d_{3/2}$ and Ce $3d_{5/2}$ principal spin-orbit states. XP spectrum for Ce showed 10 peaks, which was also confirmed by studies on CeO_2 in the literature for example, Leppelt *et al.* and Çağlayan and Aksoylu (Leppelt *et al.*, 2006-Çağlayan and Aksoylu, 2011).

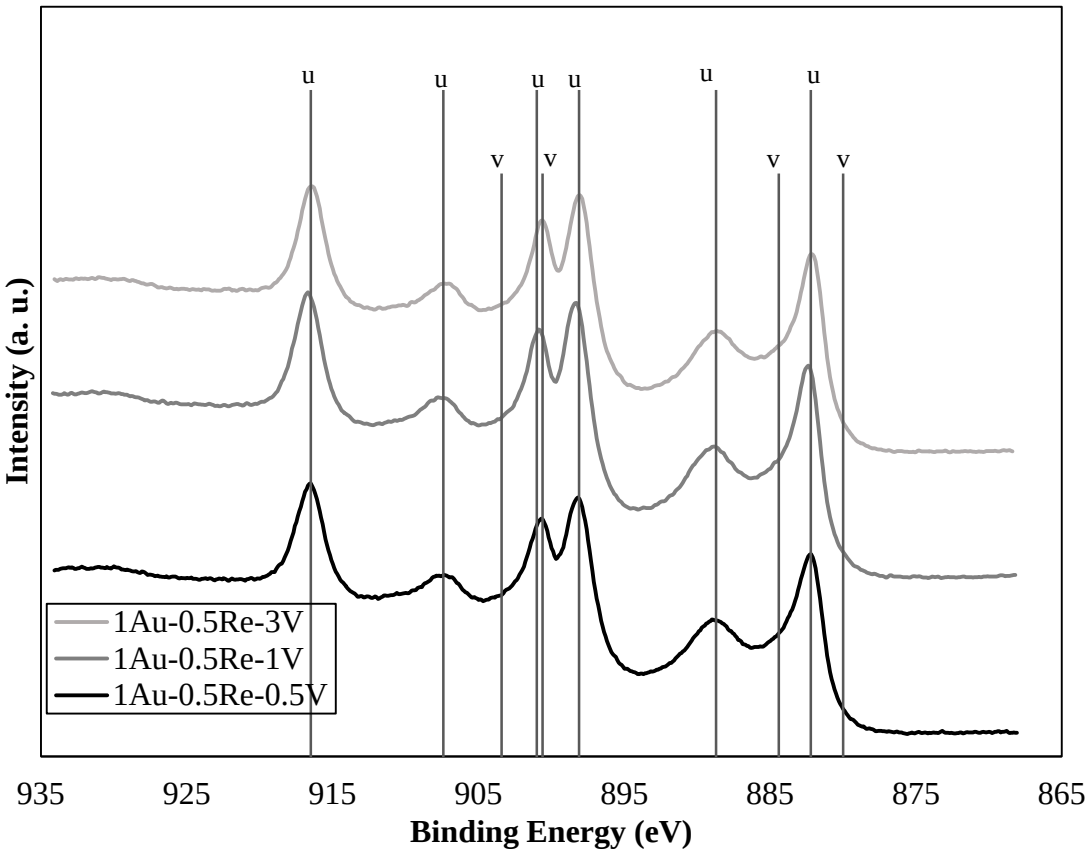

Figure 4.11. XP spectra of Ce 3d region of freshly reduced catalyst samples (v: Ce^{3+}, u: Ce^{4+}).

Figure 4.12 shows the effect of V-loading on the XP spectra of Ce 3d region for freshly reduced and spent catalysts. The spent samples were used 6 h TOS in WGS test at 400 °C under the flow of ideal feed #1. The resulting spectra indicates that the peaks corresponding to Ce^{3+} and Ce^{4+}'s are still observed in the spent catalyst samples, but their intensities are different. Note that while the intensities of Ce 3d region increased for catalysts with 0.5 wt%

V-loading upon reaction; they decreased for 3 wt% V-loading. On the other hand, the intensities showed only a slight decrease for 1 wt% V loaded sample upon reaction.

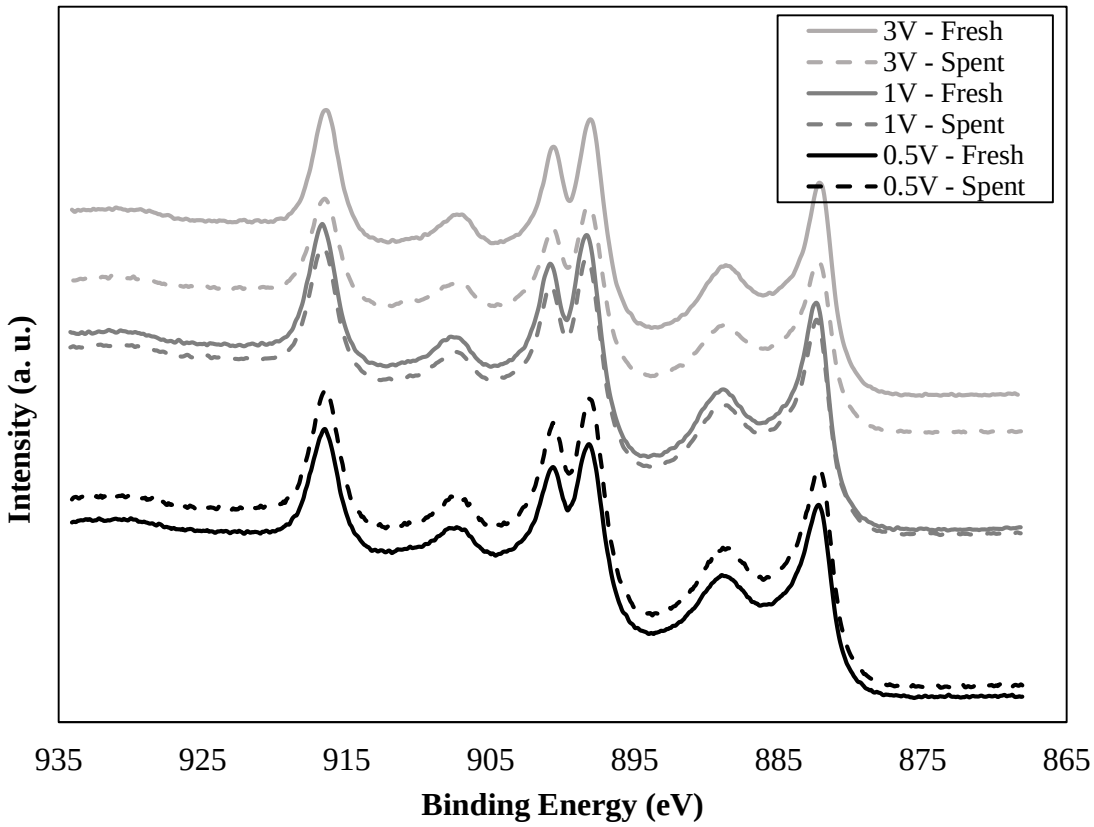

Figure 4.12. XP spectra of Ce 3d region of freshly reduced and spent (ideal feed #1, 400 °C) catalyst samples with different V-loadings.

Peak deconvolution was done via the Avantage software. Using the deconvolution results and calculated the peak areas corresponding to Ce^{3+} and Ce^{4+} regions, surface Ce^{3+} concentrations were calculated for both reduced and spent catalysts by using the following formula (Çağlayan and Aksoylu, 2011):

$$[\mathrm{Ce}^{3+}] = \mathrm{I} - \mathrm{Ce}^{3+}/(\mathrm{I} - \mathrm{Ce}^{3+} + \mathrm{I} - \mathrm{Ce}^{4+}) \tag{4.5}$$

where I – Ce^{3+} and I – Ce^{4+} represent the sum of intensities of two doublets resulting from Ce_2O_3 and three doublets resulting from CeO_2, respectively. Ce^{3+} ions on the surface correspond to the oxygen vacant defects on the surface. Ce^{3+} ions are reported to be very

reactive towards reactants in the gas phase due to excess electrons that are left behind when an oxygen atom is removed (Campbell and Peden, 2005). Ability of Ce^{3+} ions to transfer electrons from the support to metallic sites is also reported in literature (Çağlayan and Aksoylu, 2011). The Ce^{3+} contents of catalysts samples with different V-loadings are presented in Table 4.1.

Table 4.1. Effect of V-loading on Ce^{3+} contents (%) of the freshly reduced and spent catalyst samples; (ideal feed #1, and 400 °C).

Catalyst	**Ce^{3+} (%)**	
	Freshly reduced	**Spent**
1Au-0.5Re-0.5V/CeO_2	22.0	28.4
1Au-0.5Re-1V/CeO_2	17.3	21.0
1Au-0.5Re-3V/CeO_2	19.0	17.8

A comparative analysis of the Ce^{3+} content of the fresh and spent samples having different V-loading show that when the sample has low V-loading (i.e. 0.5 wt% and 1 wt %) and consequently has high WGS activity, its Ce^{3+} content increases during reaction. On the other hand, Ce^{3+} content decreases for the 3 wt% V loaded sample which showed very low activity in WGS performance tests.

In order to establish a detailed relation between the WGS activity of 0.5 wt% V loaded sample and the change in its Ce^{3+} percentage during reaction, Ce^{3+} percentage of freshly reduced 1Au-0.5Re-0.5V/CeO_2 and its spent forms tested under different reaction conditions are presented in Table 4.2.

The first two rows of Table 4.2 showed when H_2O/CO feed ratio was high, higher temperature resulted in higher increase in Ce^{3+} content during reaction. First and third rows of Table 4.2 showed that at high temperature, the reaction under high H_2O/CO feed ratio results in significant increase in Ce^{3+} percentage, while the reaction under low H_2O/CO feed ratio even results in a limited decrease. Ce^{3+} ions are most likely involved in H_2O activation; thus H_2O activation rate was higher when H_2O/CO feed ratio was high, as evidenced by

higher increase observed in Ce^{3+} content during reaction. There was no significant difference between Ce^{3+} contents of spent catalyst reacted under both realistic feeds.

Table 4.2. Ce^{3+} content (%) of 1Au-0.5Re-0.5V/CeO_2 samples for all reaction conditions; freshly reduced and spent.

Reaction Conditions (Feed – Temperature)	**Ce^{3+} (%)**	
	Freshly reduced	**Spent**
Ideal feed #1 – 400 °C	22.0	28.4
Ideal feed #1 – 250 °C	22.0	22.6
Ideal feed #2 – 400 °C	22.0	21.5
Realistic feed #1 – 250 °C	22.0	21.6
Realistic feed #2 – 250 °C	22.0	22.1

Figure 4.13 shows the effect of V-loading on the XP spectra of V 2p region for freshly reduced and spent catalysts. Peaks at 515.5, 517, and 524 eV binding energies were reported to correspond to V^{3+}, V^{5+}, and V^{5+} ions, respectively. Duarte de Farias *et al*. reported that the V^{5+} ions belonged largely to V_2O_5. V_2O_5 was reported to be inactive in WGS reaction due to presence of V–O–V bonds (Duarte de Farias *et al.*, 2008-Garcia *et al.*, 2015). Matching of the peaks showed emergence of V^{3+} ions in freshly reduced samples with the increase in V-loading. For samples with lower V-loadings, V^{3+} ions were not observed with the exception of spent sample of 1Au-0.5Re-1V/CeO_2. Duarte de Farias *et al*. similarly reported emergence of V^{3+} ions in their XPS analysis when they increased V-loading in Pt/VCeO_2 catalysts. V^{3+} ions were also reported to be inactive in WGS reaction (Duarte de Farias *et al.*, 2008).

Several studies reported formation of $CeVO_4$ phase when surface VO_x species react with the support at 400-500 °C (Martinez-Huerta *et al.*, 2008). The resulting V^{5+}–O–Ce^{3+} bonds were reported to be active for selective oxidation and WGS reactions (Duarte de Farias *et al.*, 2008- Martinez-Huerta *et al.*, 2008). The ability of $CeVO_4$ formation was attributed to stabilization of reactive Ce^{3+} sites of CeO_2 support with surface VO_x. Martinez-Huerta *et al*. conducted experiments with oxygen-18 to confirm that VO_x sites on the surface had little

reactivity and the catalytic activity was due to V–Ce interface. However, transformation of $CeVO_4$ single crystals to a more bulk crystalline phase reportedly decreased activity; mostly due to loss of number of exposed V^{5+}–O–Ce^{3+} sites on the support (Martinez-Huerta *et al.*, 2008).

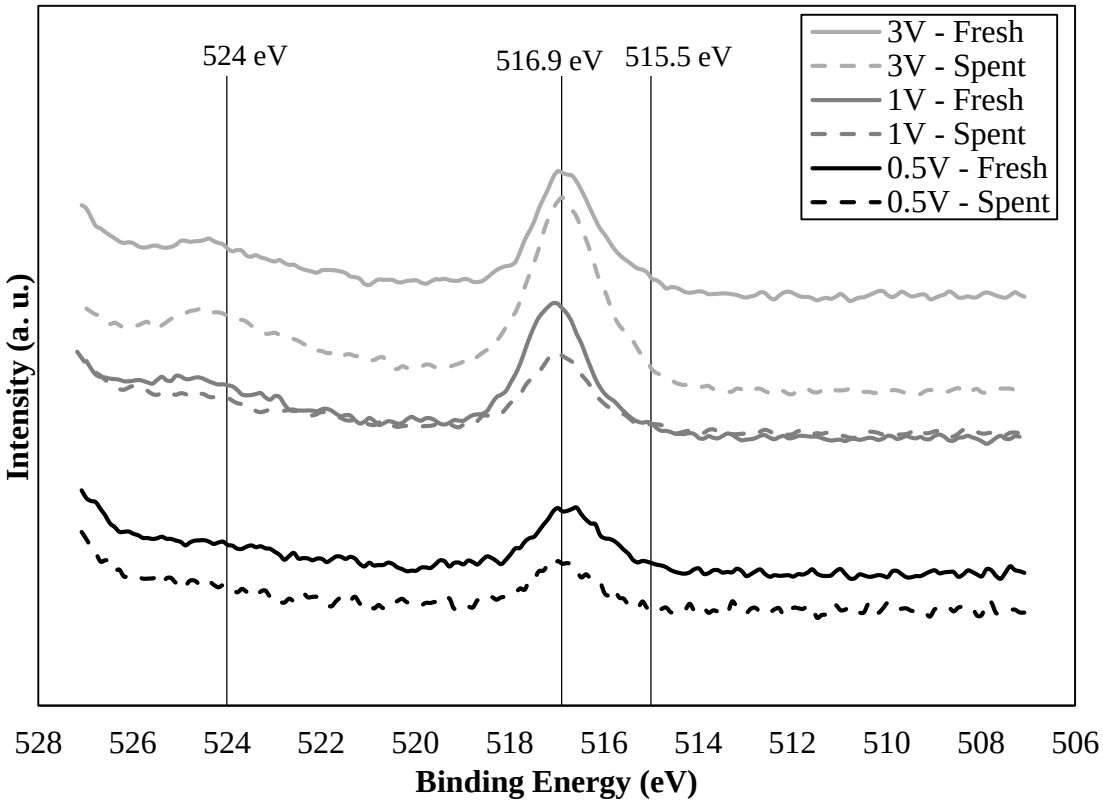

Figure 4.13. XP spectra of V 2p region of freshly reduced and spent (ideal feed #1, 400 °C) catalyst samples with different V-loadings.

Several studies reported formation of $CeVO_4$ phase when surface VO_x species react with the support at 400-500 °C (Martinez-Huerta *et al.*, 2008). The resulting V^{5+}–O–Ce^{3+} bonds were reported to be active for selective oxidation and WGS reactions (Duarte de Farias *et al.*, 2008- Martinez-Huerta *et al.*, 2008). This ability of $CeVO_4$ was attributed to surface VO_x stabilizing reactive Ce^{3+} sites on CeO_2 support. Martinez-Huerta *et al*. conducted experiments with oxygen-18 to confirm that VO_x sites on the surface had little reactivity and the catalytic activity was due to V–Ce interface. However, transformation of $CeVO_4$ single crystals to a more bulk crystalline phase reportedly decreased activity; mostly due to loss of number of exposed V^{5+}–O–Ce^{3+} sites on the support (Martinez-Huerta *et al.*, 2008).

Formation of $CeVO_4$ on Au-Re-V trimetallic catalysts was very plausible considering the calcination and reaction temperatures of 400 °C used in this work. Also, the decrease in catalytic activity when V-loading was high suggested that either V_2O_5 or bulk $CeVO_4$ were dominantly present especially in 1Au-0.5Re-3V/CeO_2. Note that, XPS analysis did not precisely conclude which phase of VO_x was present on the surface due to both V_2O_5 and $CeVO_4$ having V^{5+}.

Figure 4.14 shows the effect of V-loading on the XP spectra of O 1s region for freshly reduced and spent catalysts. Freshly reduced catalysts showed the characteristic 529, 531, and 533 eV peaks which correspond to oxygen in CeO_x lattice, chemisorbed water and hydroxyls, and weakly adsorbed water only on the CeO_x in oxidized state, respectively. It was obvious that peak at 533 eV was dramatically reduced in intensity after reaction; whereas peak at 531 eV decreased rather slightly and peak at 529 eV preserved its intensity. Çağlayan and Aksoylu observed a similar behavior in their study on 1Au-0.5Re/CeO_2. The decrease in 531 eV peak was attributed to surface hydroxyls that were spent during the reaction (Çağlayan and Aksoylu, 2011).

The decreases in 533 and 531 eV peaks were observed for all spent catalysts. Effect of temperature was examined for ideal feed #1 on 1Au-0.5Re-0.5V/CeO_2 and the results confirmed the same trends for 533 and 531 eV peaks. On the other hand, the peak at 529 eV followed a different trend; at 250 °C, the peak intensity decreased, which might be attributed to decreased rate of water activation at low temperatures resulting in decreased amount of lattice oxygen in CeO_x (Wu *et al.*, 2004).

XPS results also showed that Au was founded in its atomic Au^0 state indicated by the peaks at 83.7 and 87.7 eV (Fuggle *et al.*, 1977-Mansour, 1994). Re peaks were located at 42.3-43.6 eV, which corresponded to ReO_2 structures on the surface (Cimino *et al.*, 1980). Re was reported to be in its oxide (ReO_x) form on other CeO_2 supported catalysts (Azzam *et al.*, 2008).

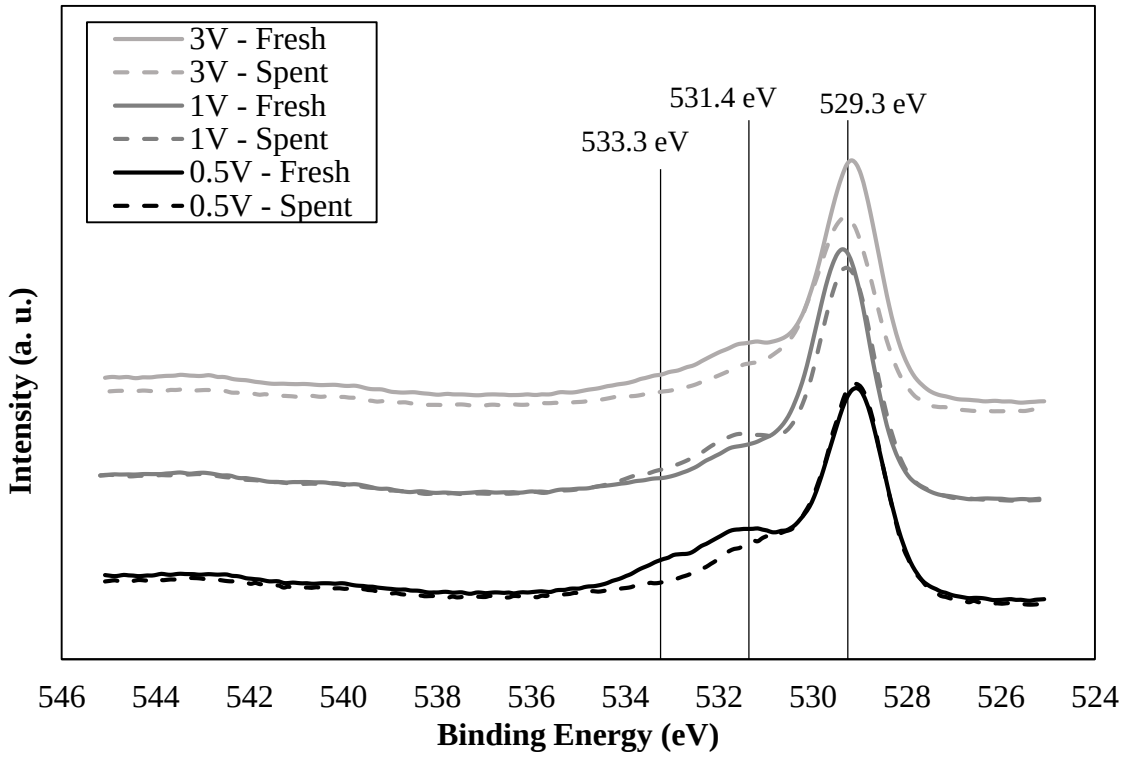

Figure 4.14. XP spectra of O 1s region of freshly reduced and spent (ideal feed #1, 400 °C) catalyst samples with different V-loadings.

4.2.3. XRD

X-ray diffraction (XRD) measurements were performed by using Cu K_α irradiation at a scan rate 2° min^{-1}. XRD spectra of the synthesized CeO_2 support, 1Au-0.5Re-3V/CeO_2, 1Au-0.5Re-1V/CeO_2, and 1Au-0.5Re-0.5V/CeO_2 catalysts are given in Figure 4.15. XRD spectra revealed that CeO_2 samples obtained in this study exhibit cerianite structure.

CeO_2 appeared to retain its cerianite structure after addition of V, Re, and Au. No diffraction peaks for V, Re, or Au were detected in the analysis. This was probably due to low (0.5-3 wt%) metal loadings and high dispersion of the metals on the CeO_2 surface. Duarte de Farias *et al.* reported emergence of V_2O_5 and $CeVO_4$ peaks in XRD analysis after V-loading was increased to 12 wt% (Duarte de Farias *et al.*, 2008).

The lattice constant and crystallite sizes for CeO_2 were calculated by using Scherrer equation as shown in Equation 4.6:

$$\tau = \frac{K\,\lambda}{\beta \cos\theta} \tag{4.6}$$

where K is the shape factor, λ is the X-ray wavelength, β is the line broadening at half the maximum intensity (FWHM) in radians,θ is the Bragg angle, and τ is the mean size of the crystallites. The lattice constants were calculated using Equation 4.7:

$$a = d\sqrt{h^2 + k^2 + l^2} \tag{4.7}$$

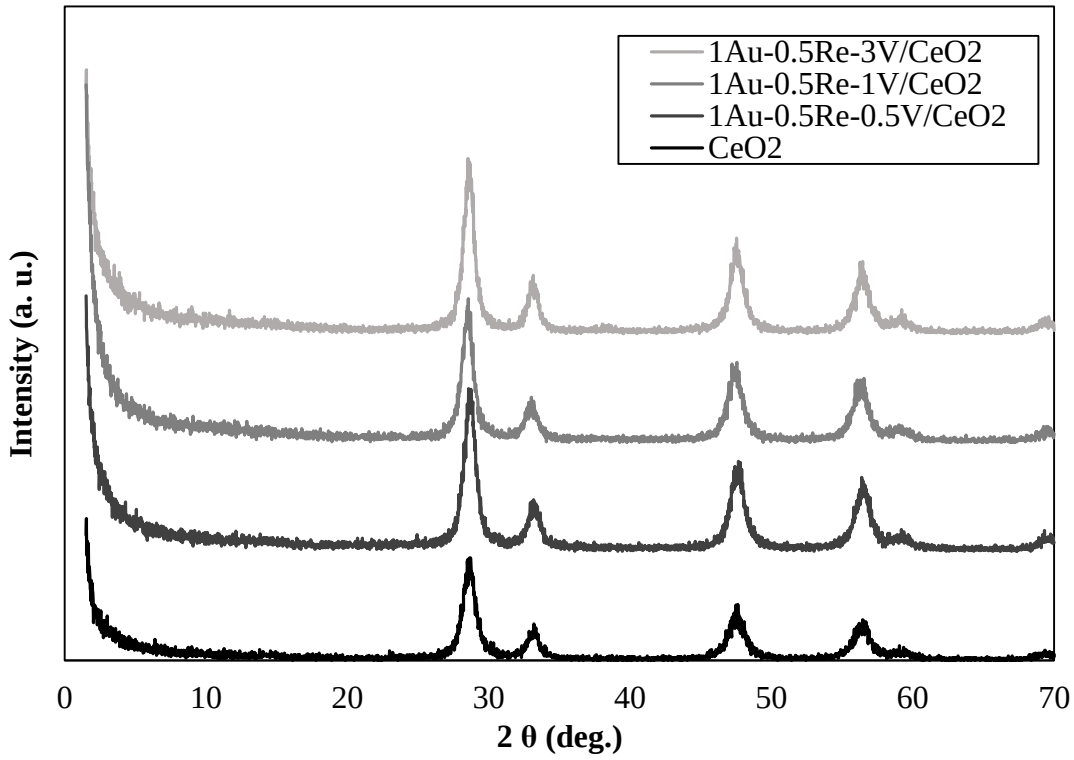

Figure 4.15. XRD spectra of the samples.

Lattice constants and crystallite sizes for CeO_2 and reduced catalysts for the diffraction peaks of the (111) plane are presented in Table 4.3.

Table 4.3. CeO_2 lattice constants and crystallite sizes of reduced samples.

Sample	**Lattice constant, a (nm)**	**Crystallite size, τ (nm)**
CeO_2	0.539	11.4
1Au-0.5Re-0.5V/CeO_2	0.539	11.6
1Au-0.5Re-1V/CeO_2	0.541	12.8
1Au-0.5Re-3V/CeO_2	0.541	12.1

Results indicated that V, Re, and Au addition to CeO_2 did not change the CeO_2 lattice constant. However, crystallite sizes were influenced by the added metal. 0.5 wt% V addition did not change the crystallite size. However, the addition of 1 wt% V increases the CeO_2 crystallite size from 11.4 to 12.8 nm. Further increase in V addition to 3 wt% led to rather limited increase compared to that observed after 1 wt % addition. These results suggested that there might be an interaction between V and CeO_2 led to a change in CeO_2 crystallite size.

4.2.4. Raman Spectroscopy

Raman spectroscopy is a method to observe vibrational, rotational, and other low frequency modes in a metal oxide system. It is considered to be the most powerful technique for characterization of surface metal oxide species (Wu *et al.*, 2011).

Figure 4.16 shows the Raman spectra for freshly reduced and spent trimetallic Au-Re-V catalysts. Spent catalysts were reacted 6 h TOS at 400 °C under the flow of ideal feed #1 having $H_2O/CO = 5$. Since the catalyst composed of mainly CeO_2 support, and CeO_2 bands are reportedly stronger in terms of signal compared to VO_x bands; the Raman spectrum was dominated by CeO_2 bands (Wu *et al.*, 2011). CeO_2 bands spotted at 460, 590 and 1175 cm^{-1}, were in accordance with the values found in the literature (Martinez-Huerta *et al.*, 2008-Wu *et al.*, 2011).

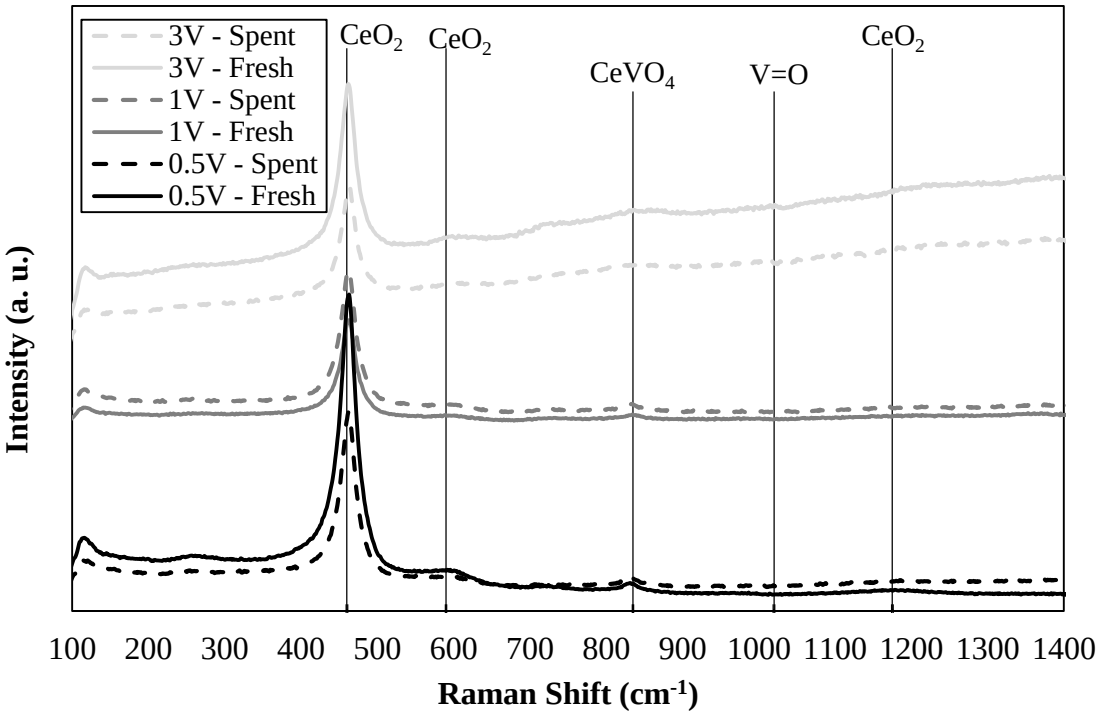

Figure 4.16. Raman spectra of freshly reduced and spent catalyst samples with different V-loadings.

V^{5+} ions were spotted in XPS analysis; however XPS analysis did not conclude whether V^{5+} ions belong to V_2O_5 or $CeVO_4$ species. The band at 830 cm^{-1} in Figure 4.16 was reported to belong to $CeVO_4$ species (Martinez-Huerta *et al.*, 2008-Wu *et al.*, 2011). V_2O_5 presence was observed in form of V=O modes that were located at 980 cm^{-1}. It must be noted that as the intensity of V=O modes were very low, it was not easy to spot them. On the other hand, $CeVO_4$ peak was still small but clearly visible. However, this does not necessarily imply that $CeVO_4$ is the main form of VO_x on the catalyst surface. The Raman results only indicate that both forms of VO_x were present on the catalyst.

Figure 4.17 displays two bands associated with carbon formation on spent 1Au-0.5Re-0.5V/CeO_2 samples at the end of 6 h TOS tests conducted at 250 and 350 °C under the flow of ideal feed #1 (H_2O/CO = 5) and realistic feed #2 (H_2O/CO = 16.2), respectively. The band at 1360 cm^{-1} was attributed to D band, which represents the disordered structural mode of crystalline carbon species. The band around 1600 cm^{-1} was attributed to G band that corresponds to graphitic carbon with high degree of symmetry (Paksoy *et al.*, 2015).

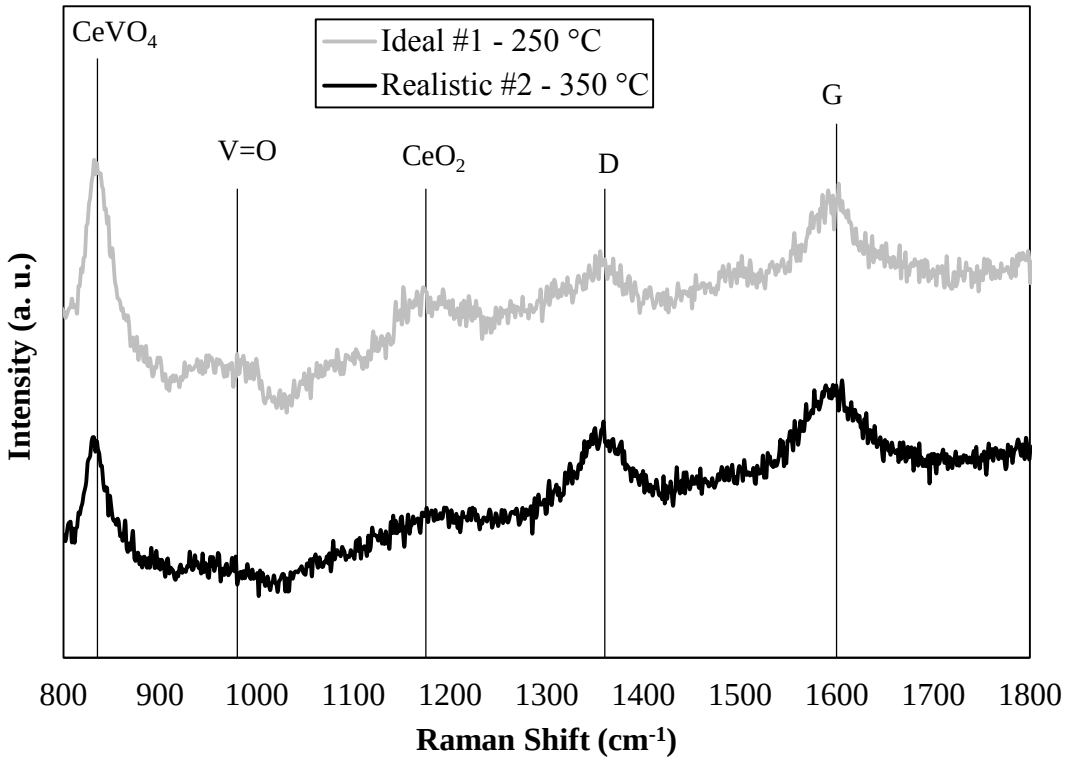

Figure 4.17. Raman spectra of spent 1Au-0.5Re-0.5V/CeO_2 catalyst samples indicating coke formation.

The performance test conducted on 1Au-0.5Re-0.5V/CeO_2 under the flow of ideal feed #1 had higher activity loss at 250 °C compared to that at 400 °C. As no coke formation was observed on the catalyst sample used in WGS test conducted at 400 °C, the formation of coke might be one of the reasons of activity loss observed during performance test conducted at 250 °C. As ideal feed #1 had H_2O/CO ratio of 5; a rough conclusion might be the improvement of H_2O activation when temperature and H_2O content of the feed are both high. The same catalyst tested under the flow of realistic feed #2 at 350 °C also experienced high activity loss which might have been caused by coke formation and depletion of surface oxygen indicated by vanishing CeO_2 peak at ca. 1175 cm^{-1}.

5. CONCLUSIONS AND RECOMMENDATIONS

5.1. Conclusions

The purpose of this experimental study was to design and develop trimetallic Au-Re-V supported over CeO_2 catalysts that suppress secondary methanation activity and show high WGS activity and stability in the temperature range of 250-400 °C under ideal and realistic feed compositions. Au- and Re-loadings were kept fixed at 1 and 0.5 wt%, respectively, while three V-loading levels, 0.5, 1, and 3 wt% were used in the trimetallic catalysts. The major conclusions of this study can be summarized as follows:

1Au-0.5Re-0.5V/CeO_2 showed highest activity and stability under all reaction conditions. Performance test results indicated that increasing V-loading in Au-Re-V system gradually decreased WGS catalytic activity and stability. 3 wt% V-promotion resulted in very low WGS activity.

For ideal feeds with low H_2O/CO ratio, activities of catalysts peaked at mid temperatures and began to decrease with further temperature increase. When H_2O/CO ratio of the ideal feed was high, the WGS activity increased with increasing reaction temperature for all catalysts suggesting suppression of reverse WGS owing to high H_2O content.

0.5 and 1 wt% V-promoted catalysts produced additional H_2 under flow of realistic feeds with high and low H_2O/CO ratios. Both catalysts had severe deactivation. High temperature improved catalytic stability, while highest additional H_2 production was obtained at mid temperature.

SEM analysis indicated that 3 wt% V-promoted sample had large sized Au clusters on the catalyst surface, which were responsible for the poor activity of 1Au-0.5Re-3V/CeO_2. Lower V-loadings resulted in well dispersed Au and Re.

XPS analysis of freshly reduced and spent samples showed that Ce^{3+} content, thus the extent of the electron transfer between the support and the metal sites, increased during

reaction as a consequence of high WGS activity. Significant increase in Ce^{3+} content at high temperature and under flow of high H_2O/CO ratio feed suggested involvement of Ce^{3+} ions in H_2O activation. Lower V-loading resulted in higher Ce^{3+} content.

XRD results indicated that V, Re, and Au addition to CeO_2 did not change the CeO_2 lattice constant. However, possible interaction between V and CeO_2 led to a change in CeO_2 crystallite size.

XPS and Raman spectroscopy results showed that V_2O_5 and $CeVO_4$ formations were both present on the catalyst. Coke formation, which was spotted on some spent samples in Raman spectroscopy, might be the cause of deactivation by depleting surface oxygen.

5.2. Recommendations

Following ideas are suggested for future studies which will use Au-Re-V/CeO_2 system or focus on other Au-based WGS catalysts:

Performing FTIR-DRIFTS studies to investigate reaction mechanisms and possible deactivation mechanisms (e.g. carbonaceous species blocking Au-O linkages).

Studying of cyclic stability of WGS catalysts during transient fuel processor operation which involves exposure of catalyst to air, liquid water, and poisonous (e.g. sulfur containing) compounds.

Designing and developing efficient start-up and shut-up down strategies for transient fuel processor operation focusing on shorter preconditioning periods.

Following catalyst compositions can be studied:

(i) Trimetallic Au-Re-V/CeO_2 system with 0.1 or 0.2 wt% V-loading,
(ii) Bimetallic Au-V/CeO_2 system,
(iii) Zr-doped CeO_2 supported single or bimetallic Au-based systems.

APPENDIX A: TIME-ON-STREAM ACTIVITY DATA

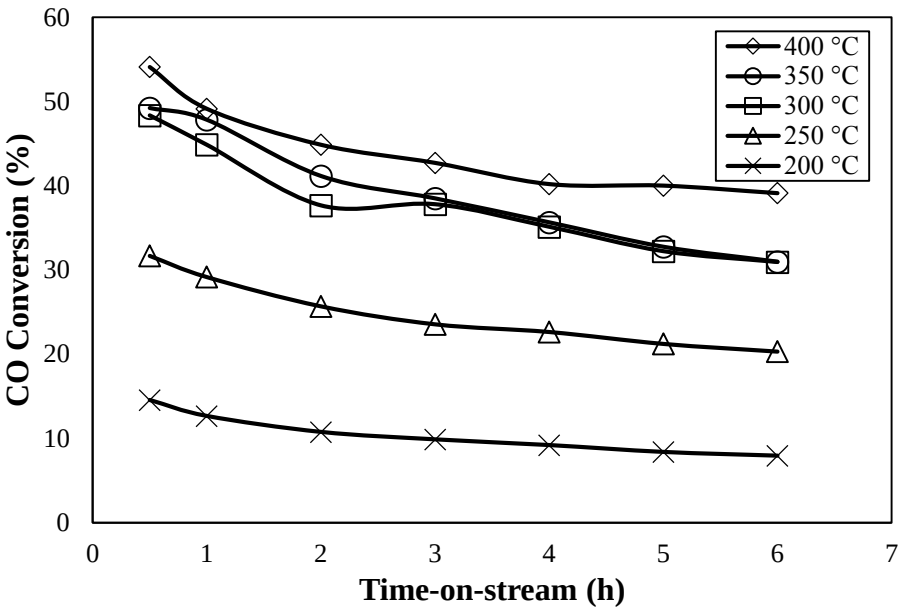

Figure A.1. Temperature dependence of time-on-stream activity data of 1Au-0.5Re-1V/CeO_2 for ideal feed #1.

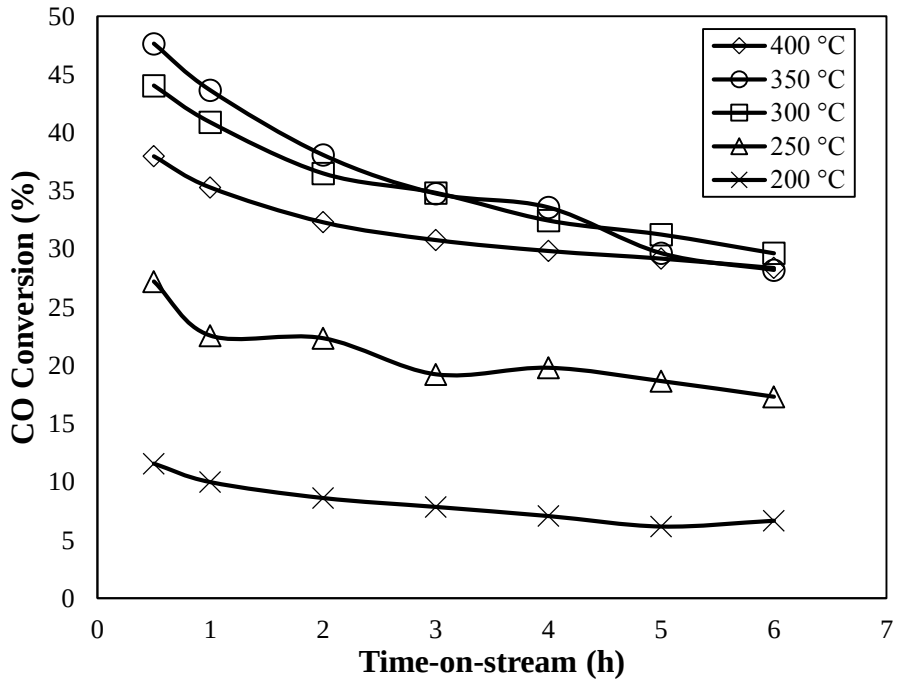

Figure A.2. Temperature dependence of time-on-stream activity data of 1Au-0.5Re-1V/CeO_2 for ideal feed #2.

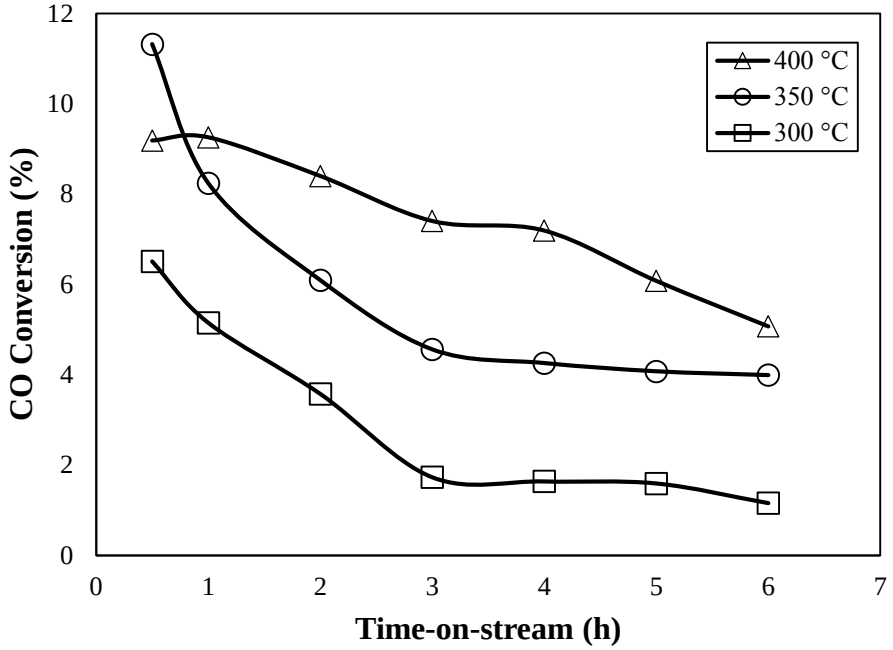

Figure A.3. Temperature dependence of time-on-stream activity data of 1Au-0.5Re-1V/CeO_2 for realistic feed #1.

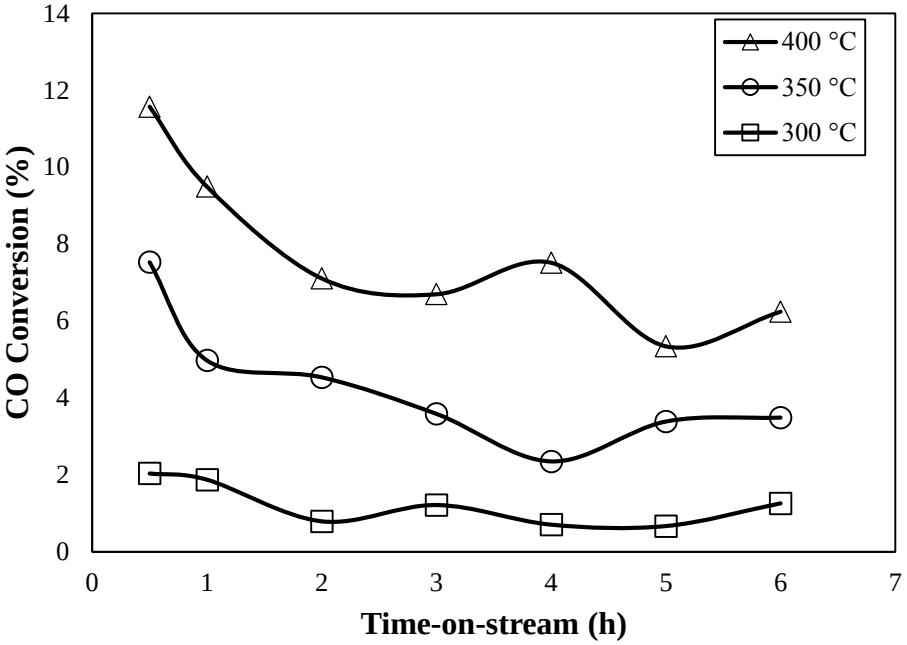

Figure A.4. Temperature dependence of time-on-stream activity data of 1Au-0.5Re-1V/CeO_2 for realistic feed #2.

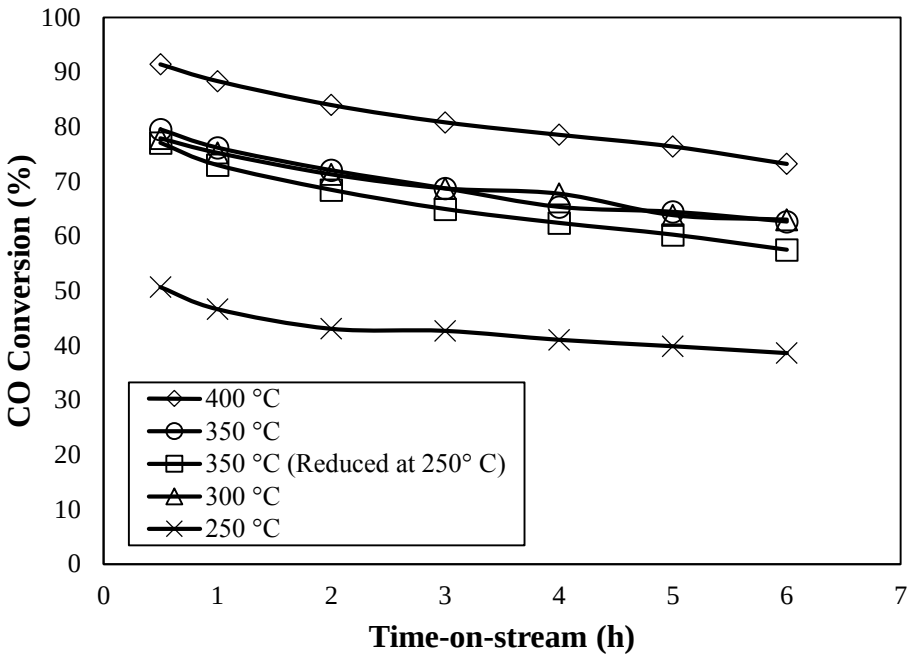

Figure A.5. Temperature dependence of time-on-stream activity data of 1Au-0.5Re-0.5V/CeO_2 for ideal feed #1.

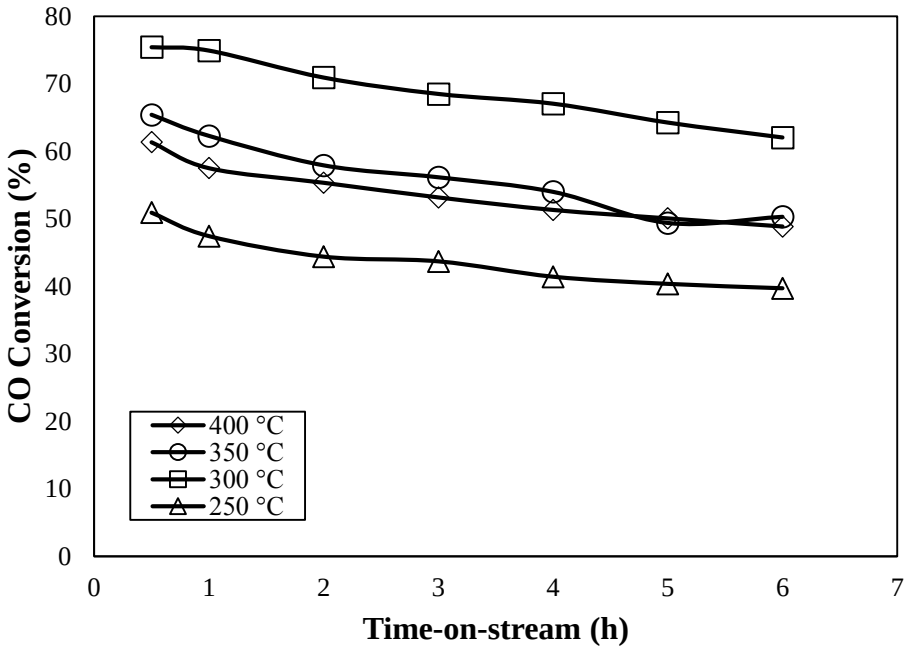

Figure A.6. Temperature dependence of time-on-stream activity data of 1Au-0.5Re-0.5V/CeO_2 for ideal feed #2.

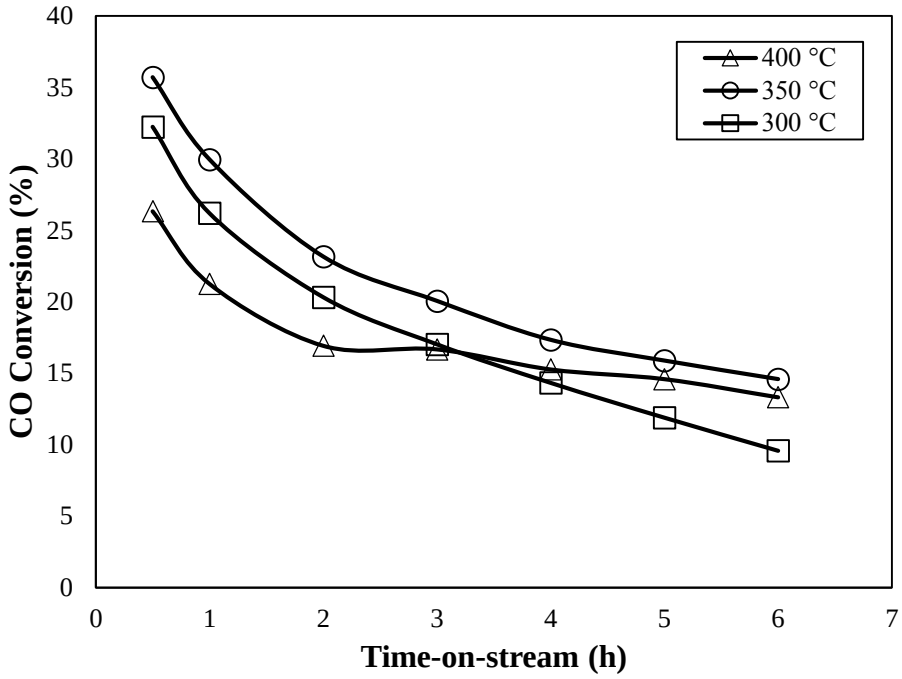

Figure A.7. Temperature dependence of time-on-stream activity data of 1Au-0.5Re-0.5V/CeO_2 for realistic feed #1.

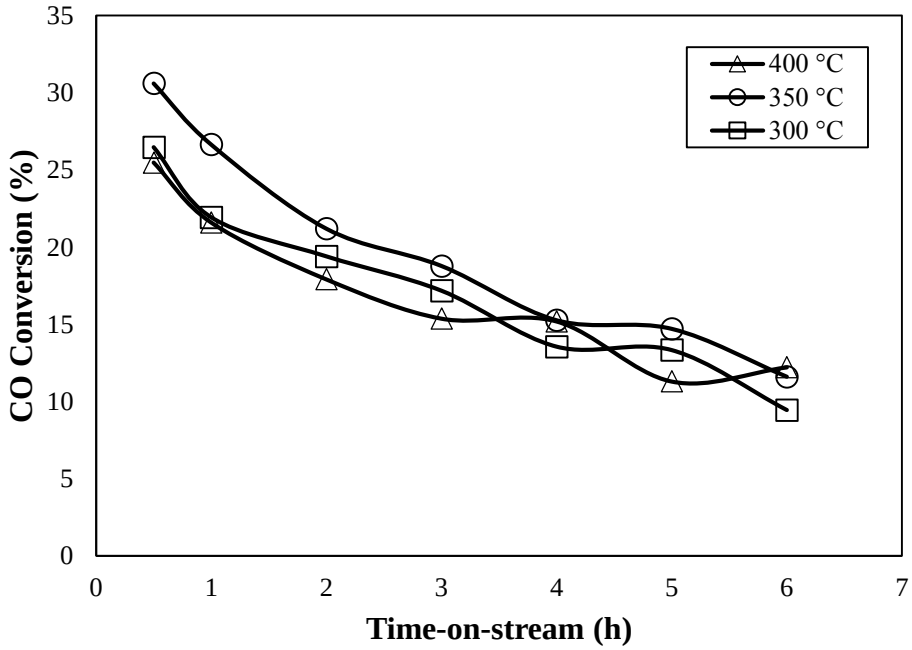

Figure A.8. Temperature dependence of time-on-stream activity data of 1Au-0.5Re-0.5V/CeO_2 for realistic feed #2.

REFERENCES

Avcı, A. K., Z. I .Önsan and D. L. Trimm, 2001, "On-board Fuel Conversion for Hydrogen Fuel Cells: Comparison of Different Fuels by Computer Simulations", *Applied Catalysis A: General*, Vol. 216, pp. 243-256.

Azzam, K. G., I. V. Babich and S. L. Leffers, 2007a, "Bifunctional Catalysts for Single-Stage Water–Gas Shift Reaction in Fuel Cell Applications. Part 1. Effect of the Support on the Reaction Sequence", *Journal of Catalysis*, Vol. 251, pp. 153–162.

Azzam, K. G., I. V. Babich and S. L. Leffers, 2007b, "A Bifunctional Catalyst for the Single-Stage Water–Gas Shift Reaction in Fuel Cell Applications. Part 2. Roles of the Support and Promoter on Catalyst Activity and Stability", *Journal of Catalysis*, Vol. 251, pp. 163–171.

Azzam, K. G., I. V. Babich, K. Seshan and L. Lefferts, 2008, "Role of Re in Pt-Re/TiO_2 Catalyst for Water Gas Shift Reaction: A Mechanistic and Kinetic Study", *Applied Catalysis B: Environmental*, Vol. 80, pp. 129-140.

Azzam, K. G., I. V. Babich, K. Seshan, B. L. Mojet and L. Lefferts, 2013, "Stable and Efficient Pt-Re/TiO_2 Catalysts for Water-Gas-Shift: On the Effect of Rhenium", *ChemCatChem*, Vol. 5, pp. 557-564.

Çağlayan, B. S. and A. E. Aksoylu, 2011, "Water–Gas Shift Activity of Ceria Supported Au–Re Catalysts", *Catalysis Communications*, Vol. 12, pp. 1206-1211.

Çağlayan, B. S., 2011, *Design and Development of Catalysts & Adsorbents for CO_x Free H_2 Production*, Ph.D. Dissertation, Boğaziçi University.

Çağlayan, B. S., İ. I. Soykal and A. E. Aksoylu, 2011, "Preferential Oxidation of CO over Pt–Sn/AC Catalyst: Adsorption, Performance and DRIFTS Studies", *Applied Catalysis B: Environmental*, Vol. 106, pp. 540-549.

Campbell, C. T. and C. H. F. Peden, 2005, “Oxygen Vacancies and Catalysis on Ceria Surfaces”, *Science*, Vol. 309, pp. 713-714.

Castaño, M. G., T. R. Reine, S. Ivanova, M. A. Centeno and J. A. Odriozola, 2014, “Pt vs. Au in Water–Gas Shift Reaction”, *Journal of Catalysis*, Vol. 314, pp. 1-9.

Cimino, A., D. Gazzoli and M. Valigi, 1980, “The Effect of the Reduction of NH_4ReO_4 Dispersed on Titanium Dioxide on the Anatase-Rutile Transformation”, *Journal of the Less Common Metals*, Vol. 75, pp. 85-88.

Duarte de Farias, A. M., P. Bargiela, M. d. G. C. Rocha and M. A. Fraga, 2008, “Vanadium-Promoted Pt/CeO_2 Catalyst for Water-Gas Shift Reaction”, *Journal of Catalysis*, Vol. 260, pp. 93-102.

Dutta, G., U. V. Waghmare, T. Baidya, M. S. Hegde, K. R. Priolkar and P. R. Sarode, 2006, “Reducibility of $Ce_{1-x}Zr_xO_2$: Origin of Enhanced Oxygen Storage Capacity”, *Catalysis Letters*, Vol. 108, pp. 162-172.

Esch, F., S. Fabris, L. Zhou, T. Montini, C. Africh, P. Fornasiero, G. Comelli and R. Rosei, 2005, “Electron Localization Determines Defect Formation on Ceria Substrates”, *Science*, Vol. 309, pp. 752-755.

Fuggle, J. C., E. Källne, L. M. Watson and D. J. Fabian, 1977, “Electronic Structure of Aluminum and Aluminum-Noble-Metal Alloys Studied by Soft-X-Ray and X-Ray Photoelectron Spectroscopies”, *Physical Review B*, Vol. 16, pp. 750-761.

Garcia, T., J. M. López, J. M. López Nieto, R. Sanchis, A. Dejoz, M. I. Vázquez and B. Solsona, 2015, “Insights into the Catalytic Production of Hydrogen from Propane in the Presence of Oxygen: Cooperative Presence of Vanadium and Gold Catalysts”, *Fuel Processing Technology*, Vol. 134, pp. 290-296.

Gökaliler, F., 2012, *Characterization and Performance Analysis of Fuel Flexible OSR-WGS Catalysts*, Ph.D. Dissertation, Boğaziçi University.

Gökaliler, F., Z. İ. Önsan and A. E. Aksoylu, 2013, "Power-Law Type Rate Expression for WGS Reaction over Au–Re/CeO_2 Catalyst under Realistic Fuel Processor Conditions", *Catalysis Communication*s, Vol. 39, pp. 70-73.

Guo, P. J., L. F. Chen, G. B. Yu, Y. Zhu, M. H. Qiao, H. L. Xu and K. N. Fan, 2009b, "Cu/ZnO-based Water-Gas Shift Catalysts in Shut-Down/Start-Up Operation", *Catalysis Communications*, Vol. 10, pp. 1252-1256.

Guo, P., L. Chen, Q. Yang, M. Qiao, H. Li, H. Li, H. Xu and K. Fan, 2009a, "Cu/ZnO/Al_2O_3 Water-Gas Shift Catalysts for Practical Fuel Cell Applications: The Performance in Shut-Down/Start-Up Operation", *International Journal of Hydrogen Energy*, Vol. 34, pp. 2361-2368.

Haruta, M., N. Yamada, T. Kobayashi and S. Iijima, 1989, "Gold Catalysts Prepared by Coprecipitation for Low-Temperature Oxidation of Hydrogen and of Carbon Monoxide", *Journal of Catalysis*, Vol. 115, pp. 301-309.

Iida, H. and A. Igarashi, 2006, "Structure Characterization of Pt-Re/TiO_2 (Rutile) and Pt-Re/ZrO_2 Catalysts for Water Gas Shift Reaction at Low-Temperature", *Applied Catalysis A: General*, Vol. 303, pp. 192-198.

IPCC, 2007, "Summary for Policymakers. In Climate Change 2007: The Physical Science Basis, Contribution of Working Group I to the Fourth Assessment Report of the Intergovernmental Panel on Climate Change*", Geneva: World Meteorological Organization/United Nations Environment Program*.

Jeong, D. W., H. S. Na, J. O. Shim, W. J. Jang, H. S. Roh, U. H. Jung and W. L. Yoon, 2014, "Hydrogen Production from Low Temperature WGS Reaction on Co-Precipitated Cu–CeO_2 catalysts: An Optimization of Cu Loading", *International Journal of Hydrogen Energy*, Vol. 39, pp. 9135-9142.

Kalamaras, C. M., S. Americanou and A. M. Efstathiou, 2011, "''Redox'' vs ''Associative Formate with –OH Group Regeneration'' WGS Reaction Mechanism on Pt/CeO_2: Effect of Platinum Particle Size", *Journal of Catalysis*, Vol. 279, pp. 287–300.

Kam, R., J. Scott, R. Amal and C. Selomulya, 2010, “Pyrophoricity and Stability of Copper and Platinum Based Water-Gas Shift Catalysts During Oxidative Shut-Down/Start-Up Operation”, *Chemical Engineering Science*, Vol. 65, pp. 6461-6470.

Kaundinya, D. P., P. Balachandra and N. H. Ravindranath, 2009, “Grid-Connected versus Stand-Alone Energy Systems for Decentralized Power—A Review of Literature”, *Renewable and Sustainable Energy Reviews*, Vol. 13, pp. 2041-2050.

Lee, D., M. S. Lee, J. Y. Lee, S. Kim, H. Eom, D. J. Moon and K. Lee, 2013, “The Review of Cr-free Fe-based Catalysts for High-Temperature Water-Gas Shift Reactions”, *Catalysis Today*, Vol. 210, pp. 2-9.

Lenite, B. A., C. Galletti and S. Specchia, 2011, “Studies on Au Catalysts for Water Gas Shift Reaction”, *International Journal of Hydrogen Energy*, Vol. 36, pp. 7750-7758.

Leppelt, R., B. Schumacher, V. Plzak, M. Kinne and R. J. Behm, 2006, “Kinetics and Mechanism of the Low-Temperature Water–Gas Shift Reaction on Au/CeO_2 Catalysts in an Idealized Reaction Atmosphere”, *Journal of Catalysis*, Vol. 244, pp. 137-152.

LeValley, T. L., A. R. Richard and M. Fan, 2014, “The Progress in Water Gas Shift and Steam Reforming Hydrogen Production Technologies – A Review”, *International Journal of Hydrogen Energy*, Vol. 39, pp. 16983-17000.

Liu, X., P. Guo, B. Wang, Z. Jiang, Y. Pei, K. Fan and M. Qiao, 2013, “A Comparative Study of the Deactivation Mechanisms of the Au/CeO_2 Catalyst for Water-Gas Shift under Steady-State and Shutdown/Start-Up Conditions in Realistic Reformate”, *Journal of Catalysis*, Vol. 300, pp. 152-162.

Liu, X., P. Guo, S. Xie, Y. Pei, M. Qiao and K. Fan, 2012, “Effect of Cu Loading on Cu/ZnO Water-Gas Shift Catalysts for Shut-Down/Start-Up Operation”, *International Journal of Hydrogen Energy*, Vol. 37, pp. 6381-6388.

Maciel, C. G., T. F. Silva, E. M. Assaf and J. M. Assaf, 2013, "Hydrogen Production and Purification from the Water–Gas Shift Reaction on $CuO/CeO_2–TiO_2$ Catalysts", *Applied Energy*, Vol. 112, pp. 52-59.

Mansour, A. N., 1994, "Gold Mg K_α XPS Spectra from the Physical Electronics Model 5400 Spectrometer", *Surface Science Spectra*, Vol. 3, 197-201.

Martinez-Huerta, M. V., G. Deo, J. L. G. Fiberro and M. A. Bañares, 2008, "Operando Raman-GC Study on the Structure – Activity Relationships in V^{5+}/CeO_2 for Catalyst Ethane Oxidative Dehydrogenation: The Formation of $CeVO_4$", *The Journal of Physical Chemistry C*, Vol. 112, pp. 11441-11447.

Maximini, M., P. Engelhardt, M. Brenner, F. Beckmann and O. Moritz, 2014, "Fast Start-Up of a Diesel Fuel Processor for PEM Fuel Cells", *International Journal of Hydrogen Energy*, Vol. 39, pp. 18154-18163.

Nishimura, S., T. Shishido, K. Ebitani, K. Teramura and T. Tanaka, 2010, "Novel Catalytic Behavior of Cu/Al_2O_3 Catalyst Against Daily Start-Up and Shut-Down (DSS)-like Operation in the Water Gas Shift Reaction", *Applied Catalyst A: General*, Vol. 387, pp. 185-194.

Nolan, M., J. E. Fearon, G. W. Watson, 2006, "Oxygen Vacancy Formation and Migration in Ceria", *Solid State Ionics*, Vol. 177, pp. 3069-3074.

Paksoy, A. İ., B. S. Çağlayan and A. E. Aksoylu, 2015, "A Sudy on Characterization and Methane Dry Reforming Performance of $Co-Ce/ZrO_2$ Catalyst", *Applied Catalysis B: Environmental*, Vol. 168-169, pp. 164-174.

Petallidou, K. C., C. M. Kalamaras, A. M. Efstathiou, 2014, "The Effect of La^{3+}, Ti^{4+} and Zr^{4+} Dopants on the Mechanism of WGS on Ceria-Doped Supported Pt Catalysts", *Catalysis Today*, Vol. 228, pp. 183-193.

Pinaeva, L. G., E. M. Sadovskaya, Y. A. Ivanova, T. G. Kuznetsova, I. P. Prosvirin, V. A. Sadykov, Y. Shuurman, A. C. van Veen and C. Mirodatos, 2014, "Water Gas Shift and

Partial Oxidation of CH_4 over CeO_2–ZrO_2(–La_2O_3) and Pt/CeO_2–ZrO_2(–La_2O_3): Performance under Transient Conditions", *Chemical Engineering Journal*, Vol. 257, pp. 281-291.

Ratnasamy, C. and J. P. Wagner, 2009, "Water Gas Shift Catalysis", *Catalysis Reviews: Science and Engineering*, Vol. 51:3, pp. 325-440.

Reina, T. R., E. Papadopoulou, S. Palma, S. Ivanonva, M. A. Centeno, T. Oannides and J. A. Odriozola, 2014, "Could an Efficient WGS Catalyst be Useful in the CO-PrOx Reaction?", *Applied Catalysis B: Enviromental*, Vol. 150-151, pp. 554-563.

Shekhawat, D., J. J. Spivey, D. A. Berry, 2011, "Fuel Cells: Technologies for Fuel Processing", *Elsevier*.

Shishido, T., S. Nishimura, Y. Yoshinaga, K. Ebitani, K. Teramura and T. Tanaka, 2009, "High Sustainability of Cu–Al–O_x Catalysts Against Daily Start-Up and Shut-Down (DSS)-like Operation in the Water–Gas Shift Reaction", *Catalysis Communications*, Vol. 10, pp. 1057-1061.

Tabakova T., G. Avgouropoulos, J. Papavasiliou, M. Manzoli, F. Boccuzzi, K. Tenchev, F. Vindigni and T. Ioannides, 2011, "CO-free Hydrogen Production over Au/CeO_2–Fe_2O_3 Catalysts: Part 1. Impact of the Support Composition on the Performance for the Preferential CO Oxidation Reaction", *Applied Catalysis B: Environmental*, Vol. 101, pp. 256-265.

Tabakova, T., F. Boccuzzi, M. Manzoli, J. W. Sobczak, V. Idakiev and D. Andreeva, 2004, "Effect of Synthesis Procedure on the Low-Temperature WGS Activity of Au/Ceria Catalysts", *Applied Catalysis B: Environmental*, Vol. 49, pp. 73-71.

Wang, T., M. D. Porosof and J. G. Chen, 2013, "Effects of Oxide Supports on the Water-Gas Shift Reaction over Pt-Ni Bimetallic Catalysts: Activity and Methanation Inhibition", *Catalysis Today*, Vol. 233, pp. 61-69.

Wu Z., A. J. Rondinone, I. N. Ivanov and S. H. Overbury, 2011, "Structure of Vanadium Oxide Supported on Ceria by Multiwavelength Raman Spectroscopy", *The Journal of Physical Chemistry C*, Vol. 115, pp. 25368-25378.

Wu, Q. H., A. Thissen, W. Jaegermann and M. Liu, 2004, "Photoelectron Spectroscopy Study of Oxygen Vacancy on Vanadium Oxide Surfaces", *Applied Surface Science*, Vol. 236, pp. 473-478.

Zhu, X., M. Shen, L. L. Lobban and R. G. Mallinson, 2011, "Structural Effects of Na Promotion for High Water Gas Shift Activity on Pt–Na/TiO_2", *Journal of Catalysis*, Vol. 278, pp. 123-132.